Pattern formation in planar DC semiconductor gas discharges

A Thesis

submitted to
Indian Institute of Science Education and Research Pune
in partial fulfillment of the requirements for the
BS-MS Dual Degree Programme

by

Divyansh Vardhan



Indian Institute of Science Education and Research Pune
Dr. Homi Bhabha Road,
Pashan, Pune 411008, INDIA.

July, 2021

Supervisor: Arijit Bhattacharyay
© Divyansh Vardhan 2021

All rights reserved

Certificate

This is to certify that this dissertation entitled Pattern formation in planar DC semiconductor gas discharges towards the partial fulfilment of the BS-MS dual degree programme at the Indian Institute of Science Education and Research, Pune represents study/work carried out by Divyansh Vardhanat Indian Institute of Science Education and Research under the supervision of Arijit Bhattacharyay, Associate Professor, Department of Physics , during the academic year 2020-2021.



Arijit Bhattacharyay

Committee:

Arijit Bhattacharyay

M.S Santhanam

This thesis is dedicated to my beloved familiy

Declaration

I hereby declare that the matter embodied in the report entitled Pattern formation in planar DC semiconductor gas discharges are the results of the work carried out by me at the Department of Physics, Indian Institute of Science Education and Research, Pune, under the supervision of Arijit Bhattacharyay and the same has not been submitted elsewhere for any other degree.



Divyansh Vardhan

Acknowledgments

I want to thank my supervisor, Professor Arijit Bhattacharyay, for his valuable guidance and constant support throughout the project. His patience and expertise helped me to try new things and learn new techniques that will be very helpful for my career. I am grateful to the IISER Pune fraternity for providing me with exposure to the way of performing scientific research and an environment conducive to learning.
I am highly thankful to my family for giving me the freedom to pursue my interests and provide constant support.

Abstract

Gas discharges, being highly nonlinear, far from equilibrium systems, are susceptible to instabilities and so emerge as good models to study phenomenon like pattern formation and spatio-temporal chaos. While these phenomena have been observed experimentally, we lack a good theoretical description. The thesis attempts to elucidate the phenomenon of pattern formation in semiconductor gas discharges. The Drift-Diffusion model is studied analytically and numerically. A new numerical technique based on the Homotopy analysis method is developed to solve the model, where the effects of gas temperature and electric current on the voltage required to sustain the discharge are studied.

Reaction-diffusion type models are derived and analyzed to find a simple theoretical description of the pattern formation in the system. While the derived models fail to reproduce observations quantitatively, we discuss the problems with the derived models and describe possible solution to achieve a more quantitatively accurate model.

Contents

Abstract **xi**

1 Preliminaries **7**

1.1 Experimental setup 7

1.2 Basic terminology 8

1.3 Drift diffusion model of gas discharges 9

1.4 Homotopy Analysis Method 12

2 1-D Drift Diffusion model of gas discharges: Stationary case **15**

2.1 1-D drift diffusion model for gas discharges: stationary case 15

2.2 Approximate solutions of stationary 1D drift diffusion model of gas discharges 18

3 Pattern formation in high ohmic semiconductor gas discharges **35**

3.1 Two component reaction diffusion model 36

3.2 Three component reaction diffusion type model 41

4 Conclusion **47**

List of Figures

1.1 Experimental setup 8

2.1 Electric field profile obtained by 7th order Homotopy analysis approximation for given values of $\mathcal{J}_{total}$ 24

2.2 Chebyshev approximation of $\exp(-\frac{1}{|x|})$ $x \in [-0.4, 0.4]$, with max error $\approx 10^{-4}$ 25

2.3 Squared Residuals at n-th iteration number 27

2.4 Current Voltage curve obtained from solving the drift-diffusion of gas discharges using iterative Homotopy analysis method. Parameter values are $L = 328,\ \gamma = 10^{-3}$ 28

2.5 Electric field profile in gas discharges as a function of space $(x) \in [-1, 1]$ and $\mathcal{J}_{total} \in [10^{-5}, 10^{-4}]$, obtained from solving stationary drift diffusion model using iterative scheme based on Homotopy analysis method 29

2.6 Current voltage characteristic for $J_{total} \in [5 \times 10^{-7}, 4 \times 10^{-6}]$ for (a) $L = 328.4$ and (b) $L = 328$ 30

2.7 Dependence of voltage required to sustain a discharge as a function of $\mathcal{J}_{total}$ and $\frac{T}{T_o}$.Where $\mathcal{J}_{total} \in [5 * 10^{-6}, 1.7 \times 10^{-5}]$ and $\frac{T}{T_o} \in [1, 1.004]$ 32

3.1 Model defined on $(-L_x^s, L_x) \times (0, L_y)$ 35

3.2 Dispersion relation obtained from the linear stability analysis of the model 3.17 44

4.1 Numerical scheme 51

4.2 Results from transient numerical solutions of Drift-Diffusion model of gas discharges coupled to Joule heating equation at $t = 10^7$(dimensionless) . . . 52

List of Tables

2.1 Convergence control parameter and corresponding squared residual at n^{th} order for $\mathcal{J}_{total} = 10^{-5}$ 23

2.2 Convergence control parameter and corresponding squared residual at n^{th} order for $\mathcal{J}_{total} = 10^{-7}$ 23

2.3 Convergence control parameter and corresponding squared residual at n^{th} order for $\mathcal{J}_{total} = 10^{-4}$ 23

Introduction

There are more things between cathode and anode than are dreamt in your philosophy

H Raether

Gas discharges have fascinated physicists and laypeople alike ever since their invention in the 19th century. Gas discharge is cold plasma with a huge temperature difference between electrons and ionized and neutral species. It is far from equilibrium system, which is susceptible to self-organization and pattern formation. Phenomena like striations, cathode spots are observed in axial gas discharges, and Turing patterns, spirals, localized structures are characteristic of planar gas discharges.

Instabilities are not desired in the tools which employ gas discharges. But planar gas discharges also have emerged as potential experimental models to study pattern formation and self-organization. The timescales of the growth of instabilities are small compared to other traditional systems, and the vast parameter space gives the freedom to study a variety of patterns.

A major roadblock in this venture is the lack of a simple theory, which explains pattern formation. The thesis attempts to develop analytical and numerical tools to study gas discharges and develop simple models to model pattern formation.

In this work we'll focus on gas-semiconductor discharges.

This chapter will first provide a brief literature review of pattern formation in gas discharges and then state the specific problems we'll be focusing on.

A brief literature review

Experimental work

Gas discharges with high ohmic semiconductor electrodes have been used and investigated as Infrared to Visible light converters.[1]. These image converters are susceptible to pattern formation. Hexagonal and stripe Turing structures, spirals and zigzag patterns, large-amplitude solitary structures[2][3][4] have been reported at appropriate parameters. These patterns manifest themselves as two-dimensional structures in the transverse plane normal discharge axis. Properties of localized structures or dissipative solitons, such as creation and destruction, interaction with each other, formation of bound states, phase transitions have been reported[5][6].
Temporal oscillations, period-doubling cascades and Spatio-temporal chaos in semiconductor gas discharges have been documented by[7][8][9]. A detailed review of experimental work on dissipative solitons in gas discharges is well documented in [10].

Theoretical work

Astrov[2] gave a semi-phenomenological reaction-diffusion type model, based on negative differential resistance, a characteristic of gas discharges, where the components were the local potential difference between discharge gap and averaged out charge density. DD Sijacic[7], showed that the type of model suggested by Astrov[2] can't be derived from first principles, and hence why the model[2] fails to provide correct predictions.
The current-Voltage curve was perturbatively elucidated near the Townsend limit(low current) by Sijacic[11], where the total current is the perturbation parameter. Supercritical, subcritical and mixed transitions were reported from Townsend discharge to glow discharge in this work.
Model suggesting thermal instability was put forward by Mokrov and Raizer[12]. We'll work on these models. When it comes to numerical simulations, Mokrov and Raizer simulated Turing patterns in one dimension[13] and two spatial dimensions[14].

Aim of the project

The thesis aims to provide new numerical tools to work with gas discharges. Numerical simulations were attempted; in fact, most of the project was spent developing codes and experimenting with different traditional numerical techniques[See Appendix], but simulations were susceptible to numerical instabilities. Hence techniques based on the homotopy analysis method are developed.
As mentioned previously, due to the wide variety of patterns that have been observed in semi-conductor gas discharges, they emerge are potential experimental tools to study pattern formation. But we don't have simple models which can be used to explain pattern formation. This thesis is also an attempt at developing and analyzing such models.

Scope of the thesis

- We will work with direct current ohmic semiconductor-gas planar gas discharges, where instabilities and pattern formation in gas discharges in the direction transverse to discharge axis are studied. The phenomenon of self-organization which occurs axially, like striations, is out of the scope of the thesis.
- Fluid model of gas discharges. The fluid model is valid at the parameters we work in.[15]. Kinetic models are not studied.
- New numerical techniques are developed in order to solve stationary 1D drift diffusion model via homotopy analysis method.
- Following [10] we'll derive models based on negative differential resistance instability and thermal instability. And we'll study the validity of these models.

We'll first define some basic terms and introduce basic concepts in the first chapter. A numerical technique based on the homotopy analysis method is introduced in the second chapter. We'll derive reaction-diffusion type models in the third chapter. Codes and numerical schemes are described in the Appendix.

Chapter 1

Preliminaries

1.1 Experimental setup

The experimental system(Figure[1.1]) is a slightly modified setup of a discharge used for fast conversion of infrared light into the visible spectrum[1], the modification being that the discharge gap is somewhat more.

The discharge gap is filled with nitrogen at pressure $p = 10^4$ - 5×10^4 Pa. One of the electrodes, mostly cathode, is made of a high ohmic semiconductor. In contrast, the other one is made of glass coated with indium tin oxide(ITO), so it is transparent to visible light. The high ohmic electrode is in contact with a gold layer. Usually, the semiconductor electrode is kept in a cryostat($T = 100$K), making its conductivity sensitive to light; hence its application as an infrared to the visible light converter. Width of gap is $d = 0.4$-10.4 mm, in contrast to the converter, which has $d = 0.1$ mm. The thickness of the semiconductor is $a = 0.25$-1.00mm, and the diameter of the column, is $D \approx 20$ mm. The voltage applied, U_o is the control parameter, but discharge at this pressure and discharge width occurs at orders of Kilo-volt. A resistor is applied in series to restrict current.

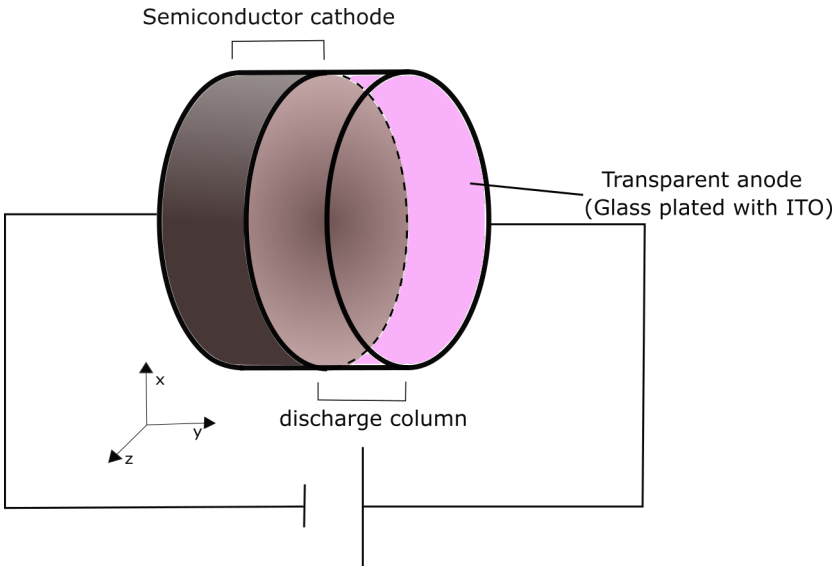


Figure 1.1: Experimental setup

1.2 Basic terminology

Townsend discharge

At low current density, the space charge in the discharge is low enough not to influence the electric field significantly, and the electric field remains spatially constant to a good approximation.

Glow discharge

Studying gas discharges as a function of current density increases current density, a transition from Townsend discharge to Glow discharge. Large gradients in profiles characterize glow discharge. There is a formation of distinct regions characterized by different intensities of glow and magnitude of the electric field.

Negative differential conductivity

A drop in voltage required to sustain a discharge when increasing current is a characteristic of the transition from Townsend to Glow discharge. $\frac{\partial V}{\partial J}$ is -ve. This property of gas discharges is called negative differential conductivity.

1.3 Drift diffusion model of gas discharges

The model to be discussed is a fluid approximation of the kinetic model of gas discharges[15]. The model comprises continuity equations for ions and electrons coupled to Poisson's equation to calculate the electric field.

Model equations

$$\begin{aligned} \partial_t n_e + \vec{\nabla} \cdot \vec{J_e} = \mathcal{S}(|\vec{J_e}|, |\vec{E}|) \quad &\| \; J_e = -n_e \mu_e \vec{E} - D_e \vec{\nabla} n_e \\ \partial_t n_i + \vec{\nabla} \cdot \vec{J_i} = \mathcal{S}(|\vec{J_e}|, |\vec{E}|) \quad &\| \; J_i = n_i \mu_i \vec{E} - D_i \vec{\nabla} n_i \\ \vec{\nabla} \cdot \vec{E} = \frac{e}{\epsilon_o}(n_i - n_e) \quad &\| \; \vec{E} = -\vec{\nabla} V \end{aligned} \tag{1.1}$$

Here, n_i, n_e denote ion and electron densities respectively, D_i, D_e are diffusion coefficients, μ_e, μ_i are mobility coefficients. $\vec{E}$ is the electric field, and V is electric potential. $\mathcal{S}$ is the local production term which depends on the magnitude of local electric field and electron flux. A widely used empirical formula for the source term suggested by Townsend is used.

$$\mathcal{S}(\vec{J_e}, \vec{E}) = |\vec{J_e}| A p \exp(-\frac{Bp}{|\vec{E}|}) \tag{1.2}$$

Here, A, B are some empirical constants that depend on the gas used, and p is gas pressure. The boundary conditions are as follows

Boundary conditions

At cathode

$$\begin{aligned} V &= 0 \\ (\vec{\nabla} n_i) \cdot \hat{n}_c &= 0 \\ \mu_e n_e &= \gamma \mu_i n_i \end{aligned}$$

Here $\hat{n}_c$ is the unit vector perpendicular to the cathode, and γ is the secondary emission coefficient, which depends on the cathode.

At anode

$$\begin{aligned} V &= V_o \\ n_i &= 0 \\ (\vec{\nabla} n_e) \cdot \hat{n}_a &= 0 \end{aligned}$$

Here $\hat{n}_a$ is the unit vector perpendicular to the anode, and V_o is the potential difference applied between the discharge.

At non-electrode walls

$$\begin{aligned} (\vec{\nabla} V) \cdot \hat{n}_w &= 0 \\ (\vec{\nabla} n_e) \cdot \hat{n}_w &= 0 \\ (\vec{\nabla} n_i) \cdot \hat{n}_w &= 0 \end{aligned}$$

where $\hat{n}_w$ is the unit vector perpendicular to the wall.

Let's discuss the model in a bit more detail. In fluid approximation, we can use the drift-diffusion model coupled to Poisson's equation to study the dynamics of electron and ion densities. It is necessary to have continuous production of electrons at the cathode to have a self-sustained discharge. This source of electrons emerges as the secondary emission of electrons from the cathode. In an ionized gas, in the presence of an electric field, ions drift towards the cathode and bombard it, and thus result in the emission of electrons from the cathode.

We have ignored the recombination processes in bulk, and only the production term is

considered. This can be rationalized from the fact that the timescale of transport of charged species in discharge is much smaller than the recombination timescales.[15]. The electrons are lost to the anode, and the ions recombine at the cathode.
Neumann boundary conditions at the walls fix the flux in and out of the domain. Dirichlet boundary condition of ions at the anode is the manifestation of the fact that ions drift away from the anode, and there is no source of ions at the anode.

1.3.1 Non-dimensionalization of the model

It is fruitful to work in particular timescales and spatial scales; hence dimensional analysis and the non-dimensionalization of the model is performed. Performing dimensional analysis on the model, the following intrinsic parameters are obtained.

$$\begin{aligned} \tau =& \frac{1}{ApBp\mu_i} \quad \xi = \frac{1}{Ap} \\ \mathcal{E}_o =& Bp \qquad\quad \eta = \frac{\epsilon_o ABp^2}{e} \end{aligned} \tag{1.3}$$

In our non-dimensionalized model, time is presented in the units of τ, which is the characteristic timescale ions take to drift for distance ξ in the electric field $\mathcal{E}_o$, spatial dimensions are measured in the units of ξ, the electric field is presented in the units of $\mathcal{E}_o$ and number density of ions and electrons is measured in the units of η
The model equations now read

$$\begin{aligned} \frac{\mu_i}{\mu_e}\partial_t \rho_e =& D_e^o \nabla^2 \rho_e + \vec{\nabla}\cdot(\rho_e \vec{\mathcal{E}}) + \rho_e |\vec{\mathcal{E}}| \exp(-\frac{1}{|\vec{\mathcal{E}}|}) \\ \partial_t \rho_i =& D_i^o \nabla^2 \rho_i - \vec{\nabla}\cdot(\rho_i \vec{\mathcal{E}}) + \rho_e |\vec{\mathcal{E}}| \exp(-\frac{1}{|\vec{\mathcal{E}}|}) \\ -\nabla^2 \mathcal{V} =& \rho_i - \frac{\mu_i}{\mu_e}\rho_e \quad \| \quad \vec{\mathcal{E}} = -\vec{\nabla}\mathcal{V} \end{aligned} \tag{1.4}$$

where

Note:All of the work in the thesis is presented in the form of non-dimensionalized model defined by Equations1.4, **??**.

1.4 Homotopy Analysis Method

The homotopy analysis method, developed by Liao[16], is a powerful technique that can be employed to solve nonlinear problems, algebraic or differential. In variance with the traditional perturbation techniques or non-perturbative techniques, firstly doesn't require any small physical parameter(a requirement by perturbative techniques), and secondly has tools that can guarantee and accelerate the convergence of the series to the solution, which the non-perturbative methods fail at. We'll introduce the basic concepts of the technique. We referred to [17],[18] for this work.

Basic concepts

Homotopy

Let X, Y be topological spaces, and $f, g: X \to Y$ be continuous maps. A **homotopy** from f to g is a continuous map $H : [0,1] \times X \to Y$ s.t

$$H(x,0) = f(x) \quad \text{and} \quad H(x,1) = g(x)\ \forall x \in X$$

If f and g can be continuously transformed into each other via varying an embedding parameter q, they are called homotopic i.e $f \sim g$. We'll refer to q as **homotopy parameter**. The concept of homotopy can be extended to algebraic and differential differential equations.

Zeroth-order deformation equation

Let $\mathcal{N}: X \to Y$ be an equation which has a solution ϕ. And $\mathcal{N}_o$ be an equation which has a solution ϕ_o.
If $\exists \quad \mathcal{H}(x,q)$ s.t $\mathcal{H}(x,q): \mathcal{N}_o(x) \sim \mathcal{N}(x)$ and $\phi_o \sim \phi$ then such $\mathcal{H}(x,q)$ is called zeroth-order deformation equation.
Note that $\mathcal{N}_o \sim \mathcal{N}$ does not necessarily imply that $\phi_o \sim \phi$. But it has been proved that if the solution of zeroth-order deformation equation converges at $q = 1$, it converges to the solution of $\mathcal{N}$[18]. Also, it hasn't been proved that a homotopy always exists, such that the solution of the zeroth order deformation equation converges.

So, we are yet attempting something that might fail, but, as we will see, we have immense freedom and flexibility to create a suitable zeroth-order deformation equation, and we have tools to check the convergence.

Homotopy-Maclaurin series

If a homotopy is appropriately constructed such that the solution of the corresponding zeroth-order deformation equation exists and is analytic at $q = 0$, then the solution of $\mathcal{H}(x, q)$ is expressed as the power series of q, known as Homotopy-Maclaurin series.

$$\phi(q) = \phi_o + \sum_{i=1}^{\infty} \phi_i q^i \tag{1.5}$$

where ϕ_i are to be determined, and are determined via i-th order deformation equations, which are defined as

$$\frac{1}{i!} \frac{\partial^i \mathcal{H}(\phi(q)}{\partial q^i}\Big|_{q=0} = 0$$

For the work ahead in this chapter, we will define $\mathcal{H}$ as

$$\mathcal{H}(\phi(q)) : (1-q)\mathcal{L}(\phi(q) - \phi_o) + \beta(q)\mathcal{N}(\phi(q)) \mid \quad \beta(0) = 0 \text{ and } \beta(1) \neq 0 \tag{1.6}$$

Where $\mathcal{L}$ is a linear operator, which we have some freedom to choose, ϕ_o is initial guess of the solution, and $\beta(q)$ has free parameters, which can control the convergence of the homotopy series. There is an immense freedom in choosing $\mathcal{L}$, ϕ_o and $\beta(q)$, and they can be chosen appropriately so as to ensure and accelerate the convergence of the homotopy series at $q = 1$.

Given 1.6 as the zeroth order deformation equation, the homotopy series is calculated via i-th order deformation equations:

$$\mathcal{L}(\phi_i - \zeta_i \phi_{i-1}) = -\frac{1}{i!} \frac{\partial^i (\beta(q)\mathcal{N}(\phi(q))}{\partial q^i}\Big|_{q=0} \quad \mid \quad \zeta_i = 1 \ \forall i \geq 2 \text{ and } \zeta_1 = 0$$

Now after obtained ϕ_i, if the homotopy series converges, we have the desired solution.
We'll use this technique to solve stationary 1D drift diffusion model in the next chapter.

Chapter 2

1-D Drift Diffusion model of gas discharges: Stationary case

In this chapter, we study the properties of the 1-D Drift-Diffusion model of gas discharges. Understanding the system's local dynamics is important to study pattern formation in planar gas discharges. Here, we use a homotopy analytic technique to solve the model, which will be defined in the following subsection.

2.1 1-D drift diffusion model for gas discharges: stationary case

Assumptions for further treatment

We have introduced the drift-diffusion model for gas discharges in the previous chapter in section1.3. For some analytical treatment, we'll make some reasonable assumptions to simplify our model. Keep in mind that all the further discussion will be in the dimensionless variables.

- Ion flux is dominated by the drift term, so the diffusive term can be ignored. So, $\vec{\mathcal{J}}_i = \rho_i \vec{\mathcal{E}}$

- $\mu_i/\mu_e \to 0$, so the electric potential is determined only by ion density, i.e

$$-\nabla^2 \mathcal{V} = \rho_i$$

- Experimentally, when the electric current is very high, the electric field becomes very low or can change the sign in some regions of the domain due to space charge effects. We'll assume that the electric field doesn't change the sign anywhere in the domain.

Keeping these assumptions in mind we'll start working on the 1D stationary case of 1.3. Using the constraint of spatial homogeneity of total current

$$\mathcal{J}_{total} = \mathcal{J}_i - \mathcal{J}_e$$

We can reduce 1.3 to two coupled equations as

$$\begin{aligned} \partial_x \mathcal{J}_i &= (\mathcal{J}_{total} - \mathcal{J}_i) \exp(-\frac{1}{\mathcal{E}}) \\ \partial_x^2(\mathcal{E}^2) &= 2\mathcal{J}_i \end{aligned} \tag{2.1}$$

with the following boundary conditions

$$\begin{aligned} \textbf{At cathode(x=L)} \quad & \mathcal{J}_i = \frac{\mathcal{J}_{total}}{(1+\gamma)} \qquad \mathcal{V} = -V_o \\ \textbf{At anode(x=0)} \quad & \mathcal{J}_i = 0 \qquad\qquad\quad \mathcal{V} = 0 \end{aligned} \tag{2.2}$$

2.1.1 Solutions at Townsend limit

Equations 2.1 are coupled nonlinear differential equations, and analytical treatment of the model is very difficult. But observe that if we assume $\partial_x^2(\mathcal{E})^2 = 2\mathcal{J}_i \approx 0$
then we can decouple the two equations.
Also, observe that we have two boundary conditions for $\mathcal{J}_i$, while the order of equation is one. This condition implies that our system is over-determined. Which only exhibits solutions when the parameters, $\mathcal{J}_{total}$ and V_o satisfy some particular relation that meets the different boundary conditions. This relation between $\mathcal{J}_{total}$ and V_o is the I-V curve of the discharge.

The solutions of 2.1 subject to boundary conditions 2.2 are

$$\begin{aligned} \mathcal{J}_{io}(x) &= \mathcal{J}_{total} - \mathcal{J}_{total} \exp\Big(- \exp(-\frac{L}{V_o})x\Big) \\ \mathcal{V}(x) &= -\frac{V_o x}{L} \end{aligned} \tag{2.3}$$

where $x \in [0, L]$ and

$$V_o = -\frac{L}{\log\big(\frac{\log(1+\gamma^{-1})}{L}\big)}$$

These solutions give a good enough description of the system at low current limit, but as current increases, charge charge effects modify the electric field profile. We will attempt to solve 2.1 and 2.2 further ahead in the chapter using Homotopy analysis method.

2.1.2 Lyapunov's artificial small parameter method

Basic concept

Given a nonlinear differential equation $\mathcal{N}(x)$ we want to solve, assume we can write $\mathcal{N}(x) = \mathcal{L}_o(x) + \mathcal{N}_o(x)$, where $\mathcal{L}_o$ is the linear part of the equation and $\mathcal{N}_o$ is the nonlinear part of the equation.

We can create a homotopy by introducing homotopy parameter q s.t $\mathcal{H}(x, q) : \ \mathcal{L}_o(x) + q\mathcal{N}_o$ Assuming we know the solution of $\mathcal{L}_o$, we can obtain the solution of the homotopy, as discussed in the previous section. As discussed previously, if the solution converges at $q = 1$, then it is the solution of $\mathcal{N}$. This technique is logically equivalent to the homotopy analysis technique but we don't have any way to guarentee the convergence of the solution.

The technique was attempted to solve equation 2.1 and 2.2, but we run into immediate problem. We want to study the model as a function $\mathcal{J}_{total}$, but since the equation governing ion current profile is of first order, and we have to satisfy the boundary conditions at each order, we can't fix $\mathcal{J}_{total}$ as a parameter and calculate V_o as a function of it. While is is possible to study the model by fixing V_o and finding $\mathcal{J}_{total}$ as a function of V_o, we'll refrain from doing so as the system exhibits multiple solutions. We'll try to solve the model via homotopy analysis technique in the next section.

2.2 Approximate solutions of stationary 1D drift diffusion model of gas discharges

In this section, we will describe a scheme based on the homotopy analysis method to solve equations 2.1 subject to boundary conditions 2.2.
We have two coupled non-linear equations.

$$\begin{aligned}
&\mathcal{N}_1(\mathcal{J}_i, \mathcal{V}) : \partial_x \mathcal{J}_i - (\mathcal{J}_{total} - \mathcal{J}_i) \exp\big(\frac{1}{\partial_x \mathcal{V}}\big) = 0 \quad x \in [0, L] \\
&\mathcal{N}_2(\mathcal{J}_i, \mathcal{V}) : \partial_x \mathcal{V} \partial_x^2 \mathcal{V} - \mathcal{J}_i = 0 \quad x \in [0, L]
\end{aligned} \tag{2.4}$$

Our goal is to obtain approximate solutions and to calculate the I-V curve. We will fix a value for $\mathcal{J}_{total}$ and calculate V_o required to sustain it. One of the issues with Lyapunov's artificial small parameter method was the inability to study the system as a function of $\mathcal{J}_{total}$.
We will define two zeroth-order deformation equation as 1.6.

$$\begin{aligned}
&\mathcal{H}_1(x, q) : (1 - q)\mathcal{L}_1(\tilde{J}_i(x, q) - J_{io}) - \beta_1(q)\mathcal{N}_1(\tilde{J}_i(x, q), \tilde{V}(x, q)) \quad \beta_1(1) \neq 0 \ , \ x \in [0, L] \\
&\mathcal{H}_2(x, q) : (1 - q)\mathcal{L}_2(\tilde{V}(x, q) - V_{io}) - \beta_2(q)\mathcal{N}_2(\tilde{J}_i(x, q), \tilde{V}(x, q)) \quad \beta_2(1) \neq 0 \ , \ x \in [0, L]
\end{aligned}$$

where we choose $\beta_1(q) = c_1 q$ and $\beta_2 = c_2 q$, where c_1, c_2 provide control over the convergence of the Homotopy-Maclaurin series obtained. The Homotopy-Maclaurin series are expressed as

$$\begin{aligned}
\tilde{J}_i(x, q, c_1, c_2) =& \mathcal{J}_{io}(x) + \sum_{n=1}^{\infty} \mathcal{J}_{in}(x, q, c_1, c_2) q^n \\
\tilde{V}(x, q, c_1, c_2) =& \mathcal{V}_o(x) + \sum_{n=1}^{\infty} \mathcal{V}_n(x, q, c_2, c_2) q^n
\end{aligned} \tag{2.5}$$

$\mathcal{J}_{io}$ and $\mathcal{V}_o$ are the initial guess solutions that satisfy the boundary conditions 2.2.

Working in polynomial basis

Further work is done in Chebyshev basis or power series basis, i.e., the solution is expressed and obtained in polynomial basis, a polynomial in x. Chebyshev polynomials are widely used to approximate continuous functions and are helpful due to their orthogonality properties.

The non-homogeneous term in $\mathcal{N}_1$, i.e the source term, will also be approximated by chebyshev basis. This is important for the feasibility of solving i-th order deformation equations to obtain $\mathcal{J}_{in}, \mathcal{V}_n$.
Chebyshev polynomials are defined on $x \in [-1, 1]$. Irrespective of the basis we choose to work with, we'll define our model on $x \in [-1, 1]$, solve the model equations become

$$\begin{aligned} \mathcal{N}_1(\mathcal{J}_i, \mathcal{V}) &: \frac{2}{L}\partial_x \mathcal{J}_i - (\mathcal{J}_{total} - \mathcal{J}_i) \exp\big(\frac{L}{2\partial_x \mathcal{V}}\big) = 0 \quad x \in [-1, 1] \\ \mathcal{N}_2(\mathcal{J}_i, \mathcal{V}) &: \frac{8}{L^3}\partial_x \mathcal{V} \partial_x^2 \mathcal{V} - \mathcal{J}_i = 0 \quad x \in [-1, 1] \end{aligned} \tag{2.6}$$

subject to following boundary conditions

$$\begin{aligned} \textbf{At cathode} \quad & \mathcal{J}_i(1) = \frac{\mathcal{J}_{total}}{(1+\gamma)} \qquad \mathcal{V}(1) = -V_o \\ \textbf{At anode} \quad & \mathcal{J}_i(-1) = 0 \qquad\quad \mathcal{V}(-1) = 0 \end{aligned} \tag{2.7}$$

Choice of auxiliary linear operators $\mathcal{L}_1$ and $\mathcal{L}_2$

Keeping in mind the boundary conditions 4.3, where we have an extra constraint on $\mathcal{J}_i(x)$ at $x = 1$ (equation for $\mathcal{J}_i$) is first-order ODE). The system is not overdetermined, and we will obtain an I-V curve when this constraint is applied. This constraint makes it impossible to study the system as a function of $\mathcal{J}_{total}$ if the auxiliary linear operator is chosen as $\mathcal{L}_1 = \partial_x$, as the literature suggests[17]. But we have freedom in choosing the operator, so, to resolve this issue, we'll choose the linear operators

$$\begin{aligned} \mathcal{L}_1 &: \partial_x^2 \\ \mathcal{L}_2 &: \partial_x^2 \end{aligned}$$

Choice of initial guess $\mathcal{J}_{io}$ and $\mathcal{V}_o$

The homotopy series will converge to the solution faster if the initial guess is close to the solution. We'll choose the initial guesses to be close to the solutions of Townsend's limit, i.e.

$\mathcal{J}_{total} \approx 0$

$$\begin{aligned}\mathcal{J}_{io}(x) =& \mathcal{J}_{total} - \mathcal{J}_{total} \exp\Big(- \exp(-\frac{L}{2\nu_o})(x+1)\Big) \\ \mathcal{V}_o(x) =& -\frac{\nu_0}{2} - \frac{\nu_o x}{2}\end{aligned} \tag{2.8}$$

where ν_o is obtained via the constraint on ion current at cathode.

$$\nu_o = -\frac{L}{\ln\Big(\frac{\ln(\frac{1+\gamma}{\gamma})}{L}\Big)}$$

Since we are working in a polynomial basis, $\mathcal{J}_{io}$ is approximated by chebyshev polynomial up-to 5th order.

n-th order deformation equations

$$\begin{aligned}\frac{1}{n!}\frac{\partial^n \mathcal{H}_1(x,q)}{\partial q^n} =& \mathcal{L}_1(\mathcal{J}_{in} - \theta\mathcal{J}_{in-1}) - \frac{c_1}{(n-1)!}\frac{\partial^{n-1}\mathcal{N}_1(\tilde{J}_i(x,q),\tilde{V}(x,q))}{\partial q^{n-1}} = 0 \\ \frac{1}{n!}\frac{\partial^n \mathcal{H}_2(x,q)}{\partial q^n} =& \mathcal{L}_2(\mathcal{V}_n - \theta\mathcal{V}_{n-1}) - \frac{c_2}{(n-1)!}\frac{\partial^{n-1}\mathcal{N}_2(\tilde{J}_i(x,q),\tilde{V}(x,q))}{\partial q^{n-1}} = 0\end{aligned}$$

where $\theta = 1\ \forall n \geq 2$ and $\theta = 0$ for $n = 1$. We'll solve for $\mathcal{J}_{in}$ and $\mathcal{V}_n$ subject to following boundary conditions

$$\begin{aligned}\mathcal{J}_{in}(1) &= 0 \qquad & \mathcal{V}_n(1) &= -\nu_n \\ \mathcal{J}_{in}(-1) &= 0 \qquad & \mathcal{V}_n(-1) &= 0\end{aligned}$$

where ν_n is calculated via constraint on ion current at cathode, given a electric field profile, ion current profile is given by

$$\mathcal{J}_i(x) = \mathcal{J}_{total} - \mathcal{J}_{total} \exp\Big(- \int_0^L \big(\exp(-\frac{1}{\mathcal{E}(x)})dx\big)\Big) \tag{2.9}$$

in order to satisfy the boundary condition at cathode, we get a constraint on $\mathcal{E}(x)$, which gives us the I-V curve.

When solving the model using homotopy analysis method, we'll implement the boundary condition 2.9 at every order.

For this we'll Taylor expand 2.9 in q about $q = 0$, solve at every order, and thereby obtain a value for ν_n

Having done this, we'll have obtained a homotopy series, which can be checked for conver-

gence. To check and optimize the convergence the convergence we'll now define squared residual function.

Squared residual function

$$\mathcal{R}(c_1, c_2) = \int_{-1}^{1} dx \Big(\big(\mathcal{N}_1(x, c_1, c_2, q = 1)\big)^2 + \big(\big(\mathcal{N}_2(x, c_1, c_2, q = 1)\big)^2 \Big) \tag{2.10}$$

$\mathcal{R}(c_1, c_2)$ gives a measure of the variance of the homotopy series at $q = 1$ from the actual solution. To optimize the convergence we'll minimize $\mathcal{R}(c_1, c_2)$ by choosing appropriate convergence control parameters c_1, c_2. To increase acceleration of computation, we'll use discrete squared residual, defined as

$$\mathcal{R}(c_1, c_2) = \frac{\Delta x}{L} \sum_{m=0}^{N} \Big(\big(\mathcal{N}_1(x_m, c_1, c_2, q = 1)\big)^2 + \big(\big(\mathcal{N}_2(x_m, c_1, c_2, q = 1)\big)^2 \Big)$$

where $N = \frac{L}{\Delta x}$, and $x_i = \{\frac{i\Delta x}{L}\}$ $i \in \{0, 1, 2, \ldots N-1, N\}$

2.2.1 Semi-numerical semi-analytical schemes based on homotopy analysis method using symbolic computational tools

In the previous section, we defined a homotopy that can be used to solve the stationary drift-diffusion model. But, the calculations get extremely difficult even at first order.
So, we'll use symbolic computational language to work with functions rather than numbers. We wrote programs in Mathematica.
Also, we'll fix the parameter values and obtain the voltage required to sustain a given current density for given values of $L,\ \gamma$.
For now, we'll fix the length of the discharge gap and the secondary emission coefficient and study the model as a function of $\mathcal{J}_{total}$

Attempt 1: Solutions up-to 7th order of homotopy series with Taylor expansion of the source term [Eq:1.2]

Scheme

- Define the variables, $\mathcal{J}_{in},\ \mathcal{V}_n$ and the parameters $L,\ \gamma,\ \mathcal{J}_{total}$ and give the values to the parameters
- Defining initial guess
- Solving the n-th order deformation equations sequentially till desired order(we performed calculations till 7th order) and truncating the obtained polynomial up to a certain order(we choose order to be 20 here), in order to simplify and accelerate the computation.
- Calculate the squared residual, and minimize it to obtain $c_1,\ c_2$
- Repeat the same steps for different value of $\mathcal{J}_{total}$

We'll fix $L = 328$ and $\gamma = 2.6 \times 10^{-3}$, which are the parameters in the experiment discussed in [19].
We solved for 3 values of $\mathcal{J}_{total}$, up-to seventh order of homotopy series, the computation becomes time consuming by seventh order($\sim$30 minutes), so higher order computations weren't performed.

Results

n	c_1	c_2	$R(c_1, c_2)$
2	527.435	92568.6	9.63715×10^{-14}
3	1708.49	916.739	1.44505×10^{-8}
5	642.531	348.171	1.46105×10^{-8}
4	3137.46	1678.25	2.28606×10^{-9}
6	1220.13	654.969	2.82623×10^{-9}
7	1.56628	114643	2.42351×10^{-15}

Table 2.1: Convergence control parameter and corresponding squared residual at n^{th} order for $\mathcal{J}_{total} = 10^{-5}$

n	c_1	c_2	$R(c_1, c_2)$
2	21.4042	107014	4.76385×10^{-20}
3	2349.12	1259.78	1.42832×10^{-12}
4	3893.69	2086.28	3.62068×10^{-13}
5	-1732.31	4503.74	1.7889×10^{-13}
6	1288.26	4556.8	2.1023×10^{-13}
7	7.98187	122084	2.7508×10^{-20}

Table 2.2: Convergence control parameter and corresponding squared residual at n^{th} order for $\mathcal{J}_{total} = 10^{-7}$

n	c_1	c_2	$R(c_1, c_2)$
2	580.274	66152.8	3.8254×10^{-10}
3	154.494	96355.7	4.7038×10^{-11}
4	365.333	45853.8	3.1871×10^{-10}
5	43.1631	75021.3	1.1615×10^{-10}
6	55.0293	62653.8	4.8509×10^{-11}
7	47.3463	56013	3.5944×10^{-11}

Table 2.3: Convergence control parameter and corresponding squared residual at n^{th} order for $\mathcal{J}_{total} = 10^{-4}$

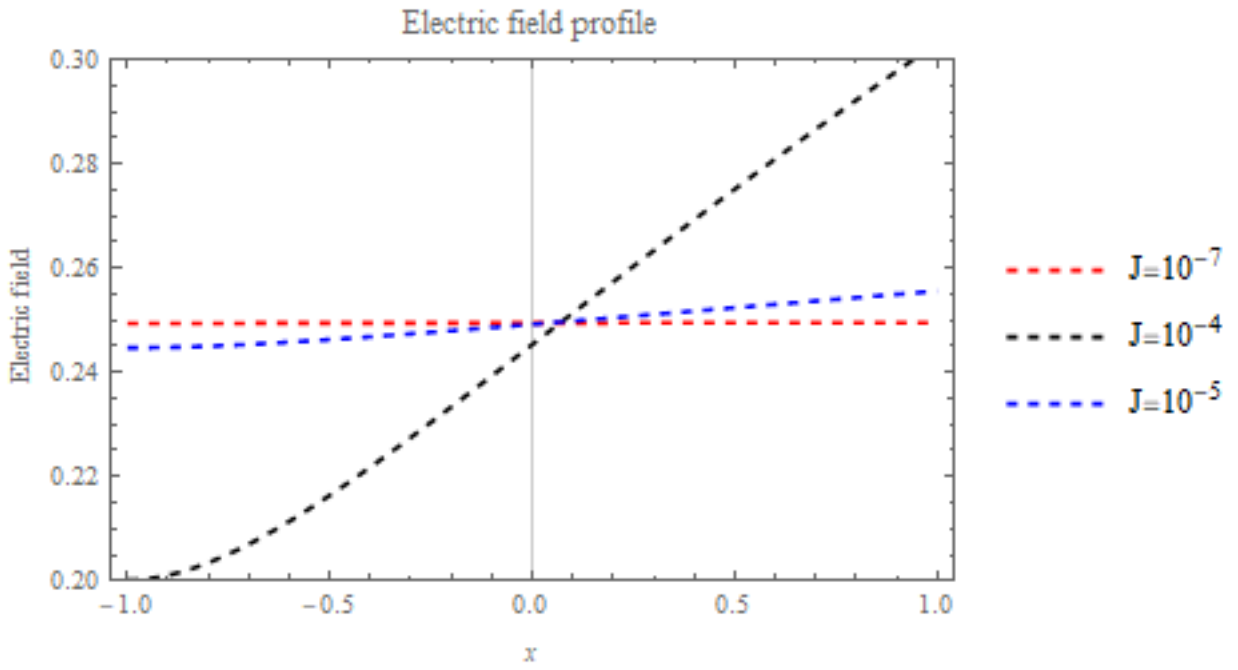


Figure 2.1: Electric field profile obtained by 7th order Homotopy analysis approximation for given values of $\mathcal{J}_{total}$

Looking at the tables [2.1,2.2,2.3] we can see that the squared residual value decreases, but it's not monotonic. At 7th order, the values of $R(c_1, c_2)$ is the lowest for the three values of the current. And the figure 2.1 shows electric field redistribution due to space charge effects. So, qualitatively, the scheme works.
But as apparent from the tables [2.1,2.2,2.3], $R(c_1, c_2)$ does not monotonically decrease, and the convergence control parameter varies a lot on varying the order of calculation. So, we can't make an inductive claim that the series obtained for a given set of convergence control parameters is actually convergent.
We'll now try and develop another, scheme which is computationally efficient.

Attempt 2: Iterative scheme based on Homotopy analysis method

Looking at the previous scheme, we observe that the value of $R(c_1, c_2)$ is low for small order approximations. We can create a scheme where we iteratively solve the model, where at each iteration, we solve up to the small order. The initial guess at each iteration is the solution of the previous iteration.

However, now, we can't use the $\exp(-\frac{1}{\mathcal{E}})$ in its original form, as the initial guesses will have some function dependence on space, and we are working in polynomial basis. We need a polynomial approximation for this term, and it is obtained by finding a Chebyshev approximation to the function.

Polynomial approximation of $\exp(-\frac{1}{\mathcal{E}})$

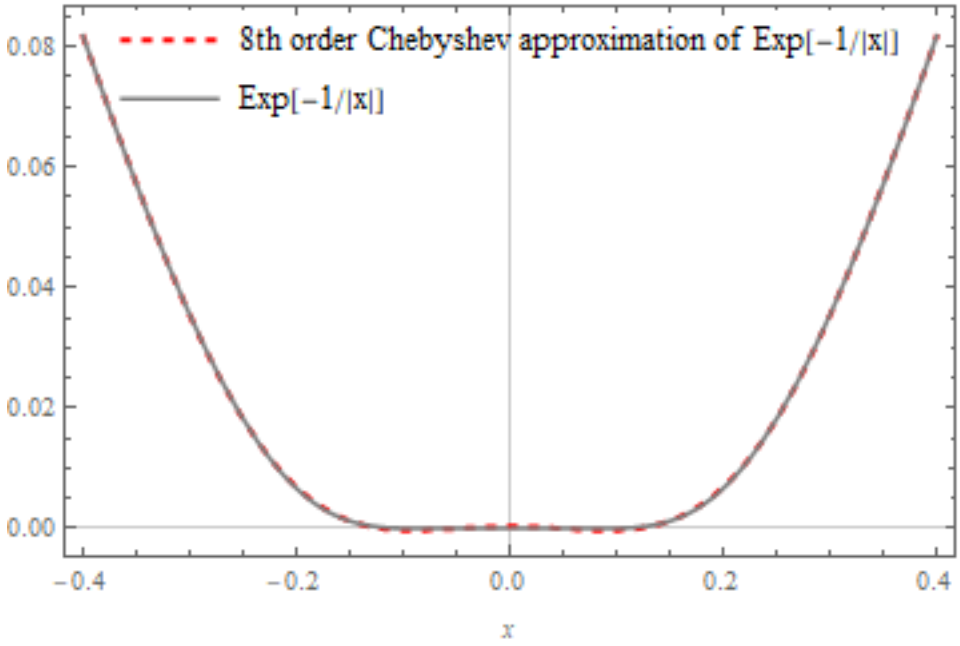


Figure 2.2: Chebyshev approximation of $\exp(-\frac{1}{|x|})$ $x \in [-0.4, 0.4]$, with max error $\approx 10^{-4}$

We will use the Chebyshev approximation of the source term in the following scheme. Since our approximate source term was calculated for $x \in [-0.4, 0.4]$, the method won't give accurate results beyond this region, i.e the validity at high electric field(~ 0.4)

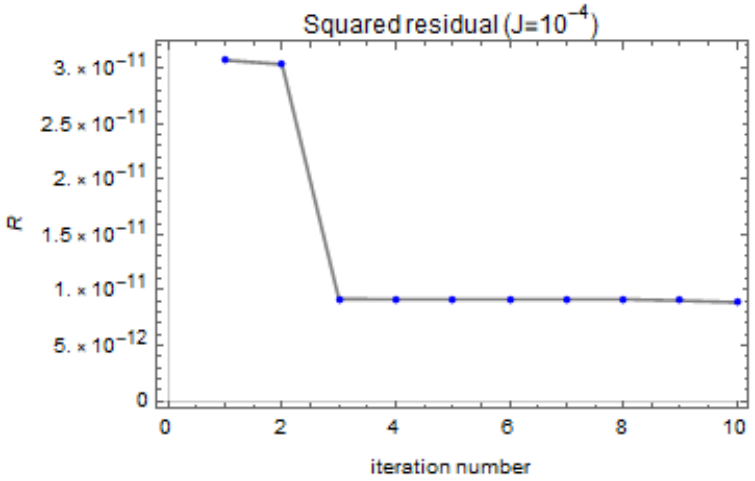
$$\begin{aligned}\exp(-\frac{1}{|x|}) \approx\ & 0.043523\left(12.5x^2 - 1.\right) + 0.00607141\left(312.5x^4 - 50.x^2 + 1.\right) \\ & - 0.00268588\left(7812.5x^6 - 1875.x^4 + 112.5x^2 - 1.\right) \\ & + 0.000448337\left(195313.x^8 - 62500.x^6 + 6250.x^4 - 200.x^2 + 1.\right) + 0.0346411\end{aligned}$$

Scheme

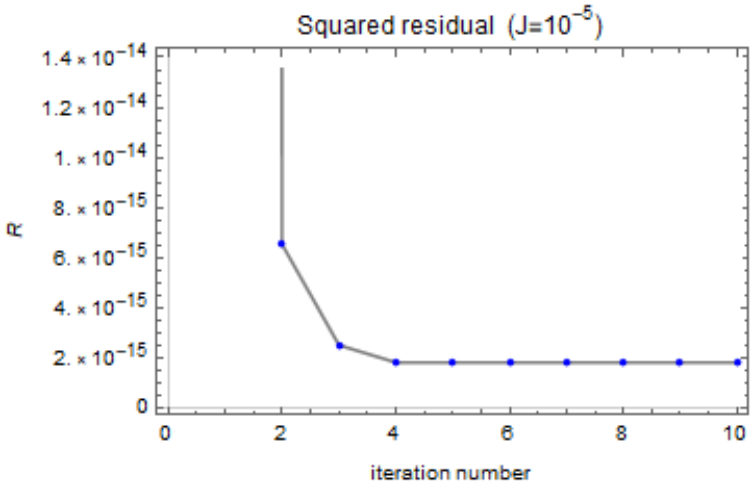
1. Define the variables, $\mathcal{J}_{in},\ \mathcal{V}_n$ and the parameters $L,\ \gamma,\ \mathcal{J}_{total}$ and give the values to the parameters
2. Defining initial guess
3. Solving the n-th order deformation equations sequentially till desired small order(2 or 3) and truncating the obtained polynomial up to a certain order(we choose order to be 20 here), in order to simplify and accelerate the computation.
4. Calculate the squared residual, and minimize it to obtain $c_1,\ c_2$
5. Define the new initial values for new iteration $\mathcal{J}_{io}$ and$\mathcal{V}_o$, as the solution obtained at this iteration
6. Repeat the steps from steps 3-5, until desired convergence is obtained
7. Repeat the same steps for different value of $\mathcal{J}_{total}$

Results

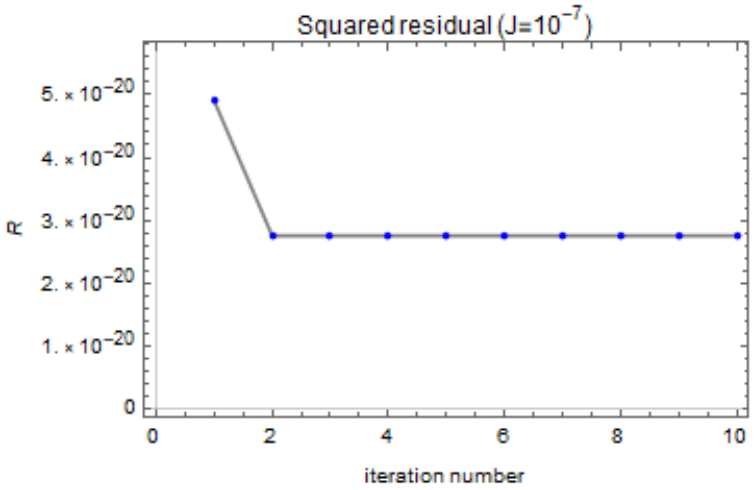
Here again we'll keep $L = 328$ and $\gamma = 2.6 \times 10^{-3}$
We again solved for 3 values of $\mathcal{J}_{total}$, $10^{-7},\ 10^{-5},\ 10^{-4}$, and referring to the results of the previous attempt, used the lowest order of homotopy approximation at each iteration. For $\mathcal{J}_{total} = 10^{-4}$ we solved up-to third order at each iteration, whereas, for the other two values of current we solved up-to second order at each iteration. Figure 2.3, shows how the squared residual changes as we increase the iteration number.
It is apparent that initial few iterations provide a steep decrease in the values of squared residual, but then the rate of decrease stagnates substantially.
Anyway, we do observe a substantial decrease in squared residual with iterations, where the squared residual decreased by $O(10^6)$ even for $\mathcal{J}_{total} = 10^{-4}$, where the squared residual is high$O(10^{-5})$for initial guess, which decreases to $O(10^{-12})$. We'll now try to study compute V_o as a function of $\mathcal{J}_{total}$ to obtain the IV curve.



(a)



(b)



(c)

Figure 2.3: Squared Residuals at n-th iteration number

Current-Voltage characteristic

As we will see in the next chapter, the current-voltage characteristic will play an essential role in understanding pattern formation in gas discharges; we used the iterative scheme to get a current-voltage curve.

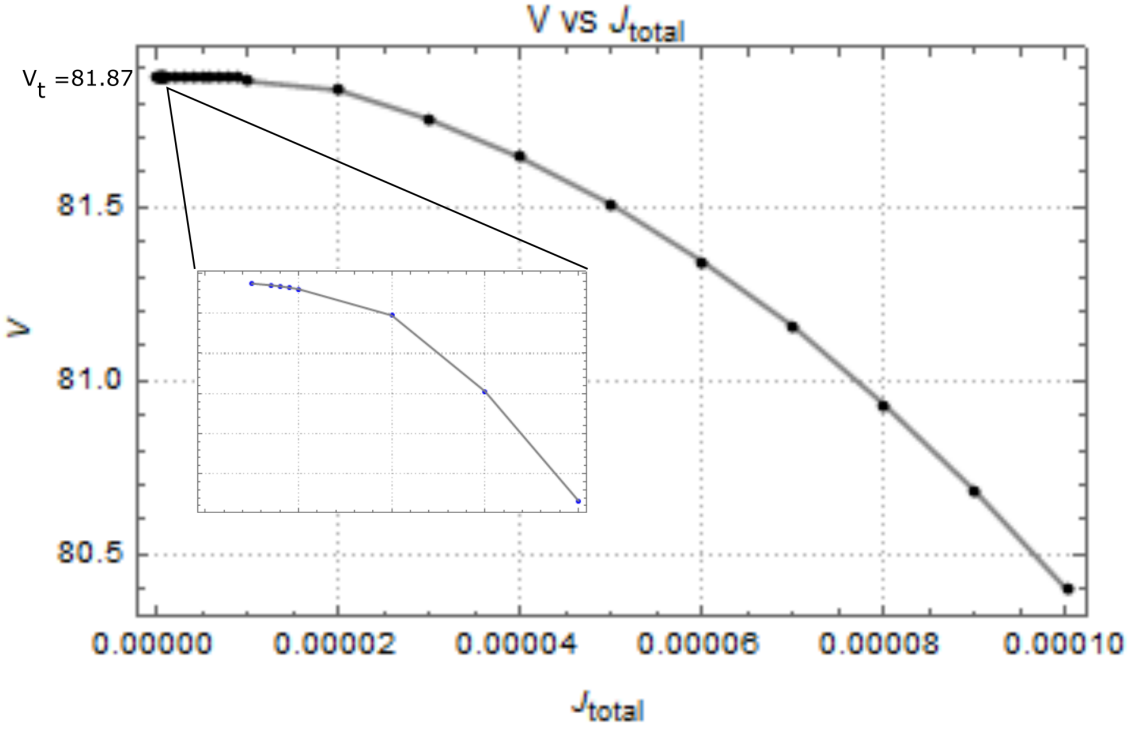


Figure 2.4: Current Voltage curve obtained from solving the drift-diffusion of gas discharges using iterative Homotopy analysis method. Parameter values are $L = 328,\ \gamma = 10^{-3}$

.

Figure 2.4 is the current-voltage characteristic obtained, using the iterative scheme. Voltage is calculated for given values of $\mathcal{J}_{total}$, where the region near $\mathcal{J}_{total} = 10^{-7}$ is finely studied, with the step size increasing as $\mathcal{J}_{total}$ is varied between 10^{-7} to 10^{-4}.
We observed a monotonic decrease in voltage required to sustain the given value of current, in the domain we are working in $[10^{-7}, 10^{-4}]$. The region of the curve where the voltage starts decreasing as the current increases shows the characteristic property of gas discharges, **negative differential resistance**(NDR)
This property of gas discharges was held responsible for the phenomena of pattern formation in planar gas discharges because, when a resistance is present in the circuit, multi-stability of

states is possible[2]. We'll study the models based on NDR which are used to study pattern formation in planar gas discharges in the next chapter.

The reason for the decrease in voltage required to sustain higher currents is the distortion of electric field due to space charge effects. Qualitatively, what happens is that, most of the ionisation happens near the cathode, due to elevated electric field near that region, and the charged particle produced here are sufficient to sustain the discharge, without needing much ionisations in rest of the domain. In the rest of the domain all electrons have to do is to drift towards anode, which requires less energy as compared to when electrons were also required to ionize in order to sustain the discharge. Since electrons are ionizing in a small region of discharge, less energy is required by electrons to sustain the discharge, hence a decrease in voltage.[20] We can also see the change in electric field profile as we vary $\mathcal{J}_{total}$ in figure 2.5.

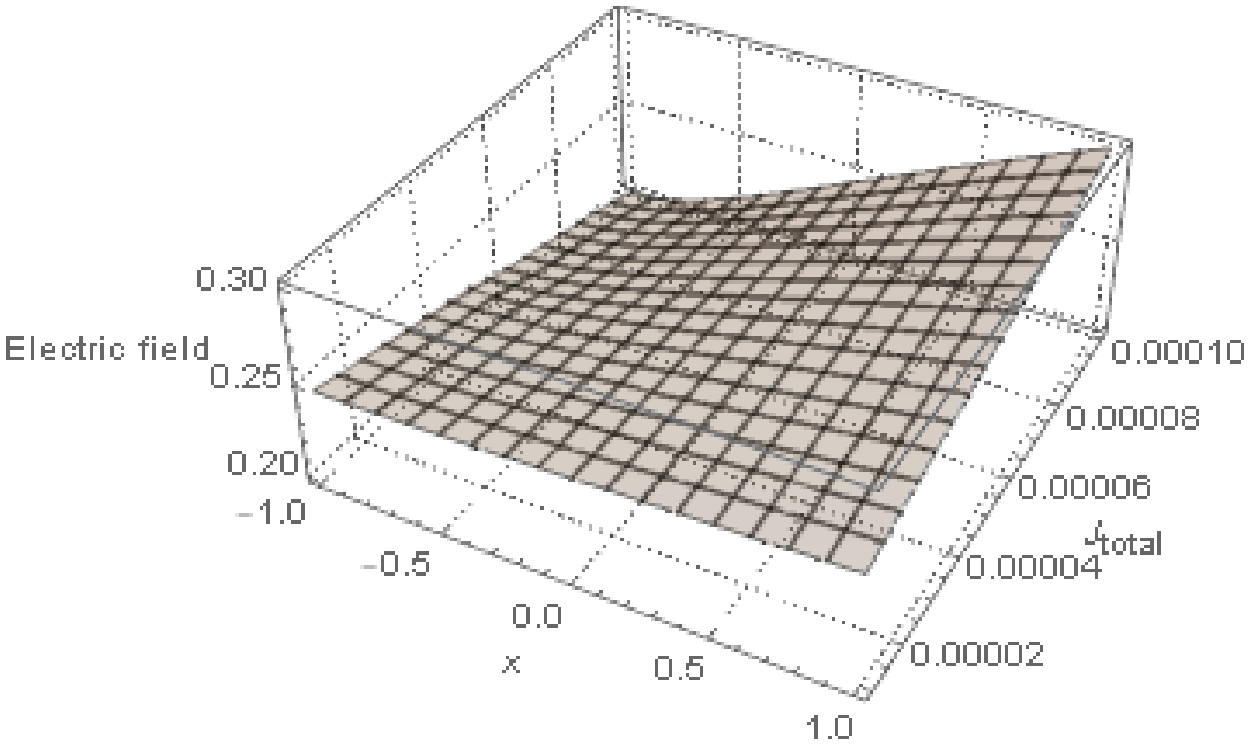
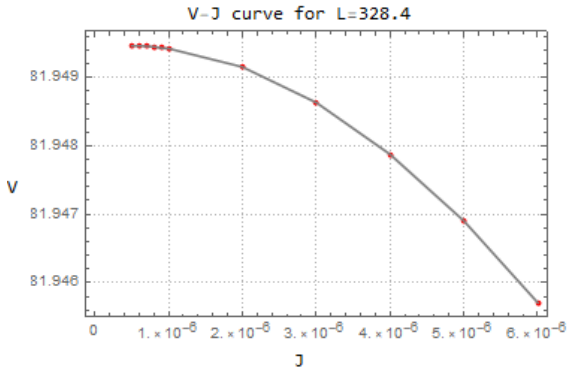


Figure 2.5: Electric field profile in gas discharges as a function of space $(x) \in [-1, 1]$ and $\mathcal{J}_{total} \in [10^{-5}, 10^{-4}]$, obtained from solving stationary drift diffusion model using iterative scheme based on Homotopy analysis method

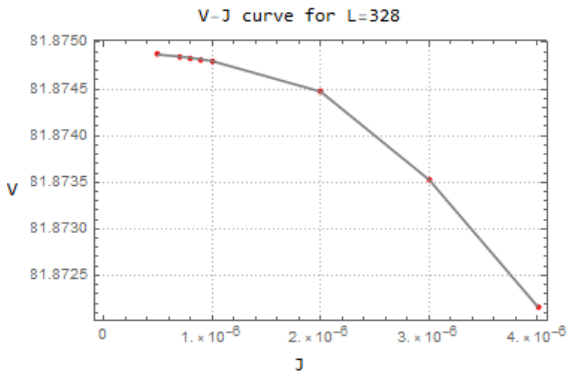
An observation from figure 2.5, the electric field increases near cathode($x = 1$) at higher values of $\mathcal{J}_{total}$ and decreases near the anode($x = -1$), this is expected, due to space charge effects.

2.2.2 Current-Voltage characteristic as a function of discharge length

We studied the model as a function of discharge gap length(L). It is intuitive that as the discharge gap decreases the voltage required to sustain the discharge also decreases. And that's what we obtain.



(a)



(b)

Figure 2.6: Current voltage characteristic for $J_{total} \in [5 \times 10^{-7}, 4 \times 10^{-6}]$ for (a) $L = 328.4$ and (b) $L = 328$

Looking at figure 2.6, we see that a small change in length of the discharge gap changes

the current voltage curve. Note that the Townsend voltage for $L = 328.4$ is 81.89 whereas for $L = 328$ it is 81.87.

2.2.3 Dependence of the model on gas temperature

Gas temperature dependency appears in the drift-diffusion model as the pressure in the source term [1.2]. As temperature varies, so does the pressure. Thus temperature changes the intrinsic parameters[1.3] of the model. Since the values of the Townsend parameter A, B are defined such that they require the value of pressure at $T = 293K$, $p \sim \frac{1}{T}$, where T is the temperature of the gas.
Using the intrinsic parameters 1.3, we see that

$$\tau \propto (\frac{T}{T_o})^2$$
$$\xi \propto \frac{T}{T_o}$$
$$\mathcal{E}_o \propto \frac{T_o}{T}$$
$$\mathcal{J}_{total} \propto (\frac{T}{T_o})^3$$

Thus current voltage curve as a function of $\frac{T}{T_o}$ varies as

$$\mathcal{V}(L, \mathcal{J}_{total}) \rightarrow \mathcal{V}\Big(L(\frac{T_o}{T}), \mathcal{J}_{total}(\frac{T^3}{T_o^3})\Big)$$

Current-Voltage-Temperature Plot

For observing the dependence of temperature on the current-voltage curve, we computed the current-voltage curves for the scaled-up discharge gap corresponding to the temperature, when varied from T_o. Then we scaled the current density with $(\frac{T}{T_o})^3$. The voltage required to sustain a discharge decreases with an increase in temperature if the current density is constant. This is because an electron requires less energy in discharge to ionize a gas atom or molecule at a higher temperature. Figure 2.7 shows the dependence of voltage required to sustain a discharge, as function of $\mathcal{J}_{total}$ and $\frac{T}{T_o}$.

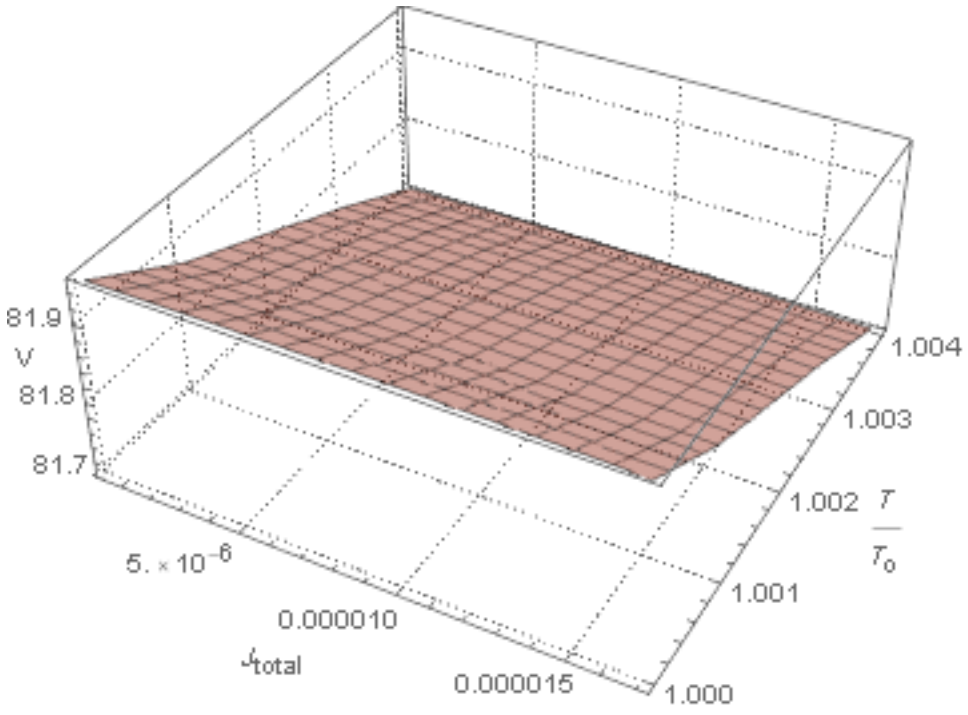


Figure 2.7: Dependence of voltage required to sustain a discharge as a function of $\mathcal{J}_{total}$ and $\frac{T}{T_o}$.Where $\mathcal{J}_{total} \in [5 * 10^{-6}, 1.7 \times 10^{-5}]$ and $\frac{T}{T_o} \in [1, 1.004]$

2.2.4 Discussion

Issues with the numerical methods developed via homotopy analysis method to solve drift diffusion model of gas discharges

- Strong dependency of the convergence control parameters on the order of computation. While the convergence control parameters are expected to vary with the order of solution, they remain close and converge to a value at higher order of computation.[18].Here looking at the tables, 2.1,2.2,2.3, we observe that the convergence control variables c_1, c_2 varies a lot as a function of n.
  We need to understand the cause behind this and check if the behavior continues for higher-order calculations.

- Saturation of squared residual as iteration number is increased. Referring to figure2.3, we observe the stagnation of the squared residual as iteration numbers are increased. This can be rather easily rationalized. The problem was with our scheme and can be removed at the cost of some computation efficiency. While writing source term as a function of the electric field, we truncated the polynomial representation of electric field at 4th order. We require higher-order approximations to get accurate results, but we also truncate at a low order to make our computations efficient. We have to truncate the polynomial at higher-order to obtain more accurate results.

- There's a major drawback to the technique we developed. Since the convergence rate of the squared residual is slow, we can't guarantee that the results we obtained are accurate, even though they reproduce the expected behavior. By solving at higher-order we may get smaller values for the squared residual, but that is computationally expensive. A more careful analysis of convergence control parameters and the choice of basis functions is required.

- Domain of the functionality of the technique is pretty restricted. We made certain assumptions at the starting of the chapter, when those assumptions don't hold, the techniques don't work.

We posited a semi-analytical technique based on Homotopy analysis method to solve stationary drift diffusion model. We were able to reproduce expected behaviour, but there are problems with the method and fundamental issues of Homotopy analysis method must

be resolved before we can go ahead. We don't know much about the convergence control parameters and the claims of convergence of the obtained series require a more deductive study.

We used a linear auxiliary operator $\mathcal{L}_1$ with the different order than of the nonlinear equation we want to solve. This is in variance with the rules suggested in [18]. But this is the freedom which homotopy analysis method provides us with.

Current-Voltage characteristic was obtained from the model and was also studied as a function of temperature of the gas. The technique is simple and elegant and this work showcases it's strength to solve highly non-linear problems. However, there are obvious issues with the technique, which should be resolved.

Future work includes formalizing the technique and providing with a more rigorous description and attempting different models to resolve the issues with the method discussed in this chapter.

Chapter 3

Pattern formation in high ohmic semiconductor gas discharges

The present chapter discusses previously proposed models developed to explain pattern formation in planar gas discharges with high ohmic semiconductor electrodes.
The models we'll be working with will be defined as illustrated in the figure 3.1.

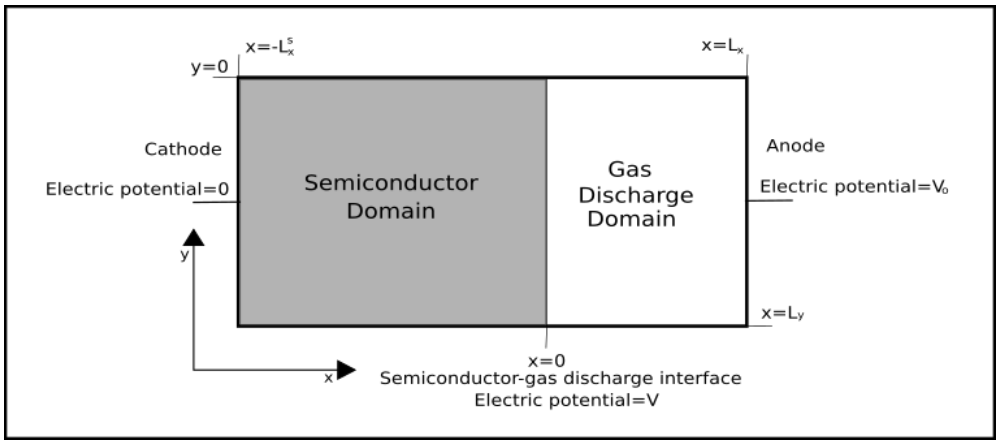


Figure 3.1: Model defined on $(-L_x^s, L_x) \times (0, L_y)$

3.1 Two component reaction diffusion model

Astrov[2], formulated a semi-phenomenological two component reaction diffusion type model in order to explain pattern formation in planar gas discharges. The Turing instability in the model was attributed to the negative differential conductivity, we discussed in previous chapter. Here we'll formulate a 1-D two component model based on the NDR, two scalar components being the axial component of electric current and the electric potential at semiconductor-gas discharge boundary. Mokrov and Raizer's work[12] was referred for present analysis.

3.1.1 Model equations

Potential at semiconductor gas discharge boundary

At the semiconductor-gas discharge boundary, where we have discontinuity of electric field due to the buildup of surface charge, the rate of surface charge buildup is proportional to the discontinuity of electric current normal to the surface at the interface. i.e

$$\begin{aligned}\rho(y) =&\big(\vec{\mathcal{E}}(x,y)|_{x\to+0} - \epsilon_{sem}\vec{\mathcal{E}}(x,y)|_{x\to-0}\big)\cdot\hat{n}_x\\ \partial_t\rho =&\big(\sigma\vec{\mathcal{E}}(x,y)|_{x\to-0} - \vec{\mathcal{J}}(x,y)|_{x\to+0}\big)\cdot\hat{n}_x\end{aligned}$$

where $\vec{\mathcal{J}}$ is the electric current, $\hat{n}_x$ is unit vector perpendicular to the gas discharge interface, directed towards the discharge. The equations give us a constraint (3.1) on electric potential(V) at $x = 0$. We'll focus on local dynamics for now.

$$\sigma\mathcal{E}_x|_- + \epsilon_{sem}\partial_t\mathcal{E}_x|_- = \mathcal{J}_x|_+ + \partial_t\mathcal{E}_x|_+ \tag{3.1}$$

we'll be assuming $\mathcal{E}|_- \approx -\frac{V_o-V}{L_x^s}$ and $\mathcal{E}|_+ \approx \frac{V}{L_x}$ .The assumptions are valid at the parameters we are interested in, i.e Townsend limit. Both the assumptions are based on the fact that the space charge effects are negligible in both the domains.[13]

$$\frac{\sigma}{L_x^s}(V_o - V) - \frac{\epsilon_{sem}}{L_x^s}\partial_t V = \mathcal{J}_x|_+ + \frac{1}{L_x}\partial_t V$$

which can be written as

$$\mathcal{T}_J \partial_t V = V_o - V - \frac{L_x^s}{\sigma}\mathcal{J}_x \qquad \Big| \ \mathcal{T} = \frac{L_x^s}{\sigma}\Big(\frac{1}{L_x} + \frac{\epsilon_{sem}}{L_x^s}\Big) \tag{3.2}$$

$\mathcal{T}_J$ gives the basic timescales of evolution of V, and V_o is voltage applied.
Now let's consider y dependence, and try to understand how in-homogeneity of V in y direction evolves. Assume that there is an in-homogeneity of V in y, which implies transverse electric field and hence non zero transverse current which is in-homogeneous in y i.e $\partial_y \mathcal{J}_y \neq 0$. Note that in semiconductor we have negligible space charge hence

$$\vec{\nabla} \cdot (\vec{\mathcal{J}}) = 0$$

where $\vec{\mathcal{J}} = \sigma\vec{\mathcal{E}}$

$$\begin{aligned} \partial_x \mathcal{J}_x =& - \partial_y \mathcal{J}_y \\ =& - \partial_y(\sigma \mathcal{E}_y) \\ =& \sigma \partial_y^2 \delta V \end{aligned}$$

we need an estimate of the axial component of current in the semiconductor due to the in-homogeneity of V. We will average out the values of the semiconductor length. But note that we can't have a non-zero transverse component of electric field near cathode-semiconductor boundary, because cathode is a good conductor. We assume linear variation in the y component of the electric field in semiconductor, considering the low conductivity, with it being zero at cathode. Using this we get that in-homogeneity of electric potential, δV at $x = 0$ along transverse directions results in change in axial component of current as

$$\delta \mathcal{J}_x = -\frac{\sigma L_x^s}{2}\partial_y^2 V \tag{3.3}$$

Using 3.3 and 3.2, we obtain a reaction diffusion type equation 3.4 for electric potential at $x = 0$, we $\mathcal{J}_x$ appearing in the reaction term. We'll now try to find equation governing dynamics of $\mathcal{J}_x|_+$. For the sake of simplicity for future analysis, we denote $\mathcal{J}_x|_+$ with $\mathcal{J}_o$

$$\mathcal{T}_V \partial_t V = V_o - V - \frac{L_x^s}{\sigma}\mathcal{J}_o + \frac{(L_x^s)^2}{2}\partial_y^2 V \qquad \Big| \ \mathcal{T}_V = \frac{L_x^s}{\sigma}\Big(\frac{1}{L_x} + \frac{\epsilon_{sem}}{L_x^s}\Big) \tag{3.4}$$

Electric current at semiconductor gas discharge interface

Having obtained a reaction-diffusion type equation 3.4 for potential at $x = 0$, which has $\mathcal{J}_o$ in the reaction component, which is the value of electric current at $x = 0$. We'll try to find a governing dynamical equation for $\mathcal{J}_o$. First let's focus on local dynamics.
Consider that at $t = t_o$, we have electron current at $x = 0$ as $\mathcal{J}_{eo}(t)$. These electrons will drift towards cathode while ionizing more atoms and producing equal number of ions and electrons. The ions will drift towards cathode and cause secondary emission of electrons.Hence at $t = t_o + \Delta t$ we have

$$\mathcal{J}_{eo}(t_o + \Delta t) = \mathcal{J}_{eo}(t_o)\gamma(\exp(\int_0^{L_x} dx \exp(-\frac{1}{\mathcal{E}(x, \mathcal{J}_{eo})})) - 1) \tag{3.5}$$

The term in brackets in the RHS of 3.5, is the number of ions which are produced by $\mathcal{J}_{eo}$ in Δt, which drift towards cathode. At $x = 0$, the ionic current varies from electron current by a multiplying factor. The total current also follows the same recurrence relation as 3.5. Δt is the characteristic time ions take to drift along the discharge.
Assuming that Δt is much smaller as compared the time it takes for instability to develop, which is true, as we will see later in the chapter. Expanding 3.5 up to first order of Δt we obtain

$$\partial_t \mathcal{J}_o = \frac{\gamma(\exp(\int_0^{L_x} dx \exp(-\frac{1}{\mathcal{E}(x,\mathcal{J}_o)})) - 1) - 1}{\Delta t}\mathcal{J}_o \tag{3.6}$$

$\partial_t \mathcal{J}_o = 0$ when the current voltage characteristic is satisfied. Hence we can expand the RHS about the current voltage characteristic($\mathcal{V}(\mathcal{J}_o)$). We obtain

$$\partial_t \mathcal{J}_o = \frac{(1+\gamma)\log(1+\frac{1}{\gamma})L_x}{\Delta t}\Big(\frac{V - \mathcal{V}(\mathcal{J}_o)}{\mathcal{V}^2(\mathcal{J}_o)}\Big)\mathcal{J}_o$$

At the current values we see pattern formation, we are close to the Townsend limit i.e negligible space charge effects, and using perturbative analysis[See appendix] we get $\mathcal{V}(\mathcal{J}) \approx V_t + \mathcal{F}(\gamma, L_x)\mathcal{J}^2$. Where V_t is Townsend voltage Using this expression for $\mathcal{V}(\mathcal{J}_o)$ we get

$$\frac{\Delta t}{(1+\gamma)\log(1+\frac{1}{\gamma})L_x}\partial_t \mathcal{J}_o = \Big(\frac{V - V_t - (\frac{2V-V_t}{V_t})\mathcal{F}\mathcal{J}_o^2}{V_t^2}\Big)\mathcal{J}_o \tag{3.7}$$

we also need an expression for Δt, which is basically of the order of the time ions take to drift across the discharge gap. Following [21], we get

$$\begin{aligned}\Delta t =& \Big(1 - \frac{1}{\log(1+\gamma^{-1})}\Big)\frac{L_x}{\mathcal{E}} \\ \approx& \Big(1 - \frac{1}{\log(1+\gamma^{-1})}\Big)\frac{L_x^2}{V_t}\end{aligned}$$

putting all this together we get

$$\mathcal{T}_J \partial_t \mathcal{J}_o = \Big(\frac{V - V_t - (\frac{2V-V_t}{V_t})\mathcal{F}\mathcal{J}_o^2}{V_t}\Big)\mathcal{J}_o \quad \Big| \; \mathcal{T}_J = \frac{\Big(1 - \big(\log(1+\gamma^{-1})\big)^{-1}\Big)L_x}{(1+\gamma)\log(1+\frac{1}{\gamma})} \tag{3.8}$$

Now let's check how in-homogeneity in transverse direction evolves. In-homogeneity in transverse direction, implies in-homogeneity in electron density. That means that electrons diffuse into the regions with less current density. These electrons ionize more atoms under the influence of electric field and lead to increase in current. Effectively current diffuses, with the diffusion coefficient $D_J = D_e \frac{\mu_i}{\mu_e}$, as chosen in [12].
We'll highlight this point as, a wrong value of diffusion coefficient can provide with wrong results. So, careful analysis of the choice of this diffusion coefficient is required. Keeping this in mind, we write the equation governing the dynamics of current.

$$\mathcal{T}_J \partial_t \mathcal{J}_o = \Big(\frac{V - V_t - (\frac{2V-V_t}{V_t})\mathcal{F}\mathcal{J}_o^2}{V_t}\Big)\mathcal{J}_o + D_J \partial_y^2 J_o \quad \Big| \; \mathcal{T}_J = \frac{\Big(1 - \big(\log(1+\gamma^{-1})\big)^{-1}\Big)L_x}{(1+\gamma)\log(1+\frac{1}{\gamma})} \tag{3.9}$$

Equations 3.4 and 3.9 form the two component reaction diffusion type model:

$$\begin{aligned}\mathcal{T}_V \partial_t V =& V_o - V - \frac{L_x^s}{\sigma}\mathcal{J}_o + (L_x^s)^2 \partial_y^2 V \quad \Big| \; \mathcal{T}_V = \frac{L_x^s}{\sigma}\Big(\frac{1}{L_x} + \frac{\epsilon_{sem}}{L_x^s}\Big) \\ \mathcal{T}_J \partial_t \mathcal{J}_o =& \Big(\frac{V - V_t - (\frac{2V-V_t}{V_t})\mathcal{F}\mathcal{J}_o^2}{V_t}\Big)\mathcal{J}_o + D_J \partial_y^2 J_o \quad \Big| \; \mathcal{T}_J = \frac{\Big(1 - \big(\log(1+\gamma^{-1})\big)^{-1}\Big)L_x}{(1+\gamma)\log(1+\frac{1}{\gamma})}\end{aligned} \tag{3.10}$$

Linear stability analysis of the two component model (3.10)

We'll fix the parameters to be

$$\begin{aligned} L_x^s &= 746 & L_x &= 328 \\ \gamma &= 2.6 \times 10^{-3} & \sigma &= 5.06 \times 10^{-5} \end{aligned}$$

we find that $\mathcal{T}_V \gg \mathcal{T}_J$(See equations 3.18). So the dynamics happen at the scale of $\mathcal{T}_V$. So, we can assume that $\frac{\mathcal{T}_J}{\mathcal{T}_V} \approx 0$. Now we'll perform linear stability analysis and study the dynamics of different wave-modes and obtain the following dispersion relation $\omega(k)$.

$$\omega(k) = -1 - (L_x^s)^2 k^2 - \frac{L_x^s}{\sigma} \frac{J_o V_t - 2\mathcal{F}\mathcal{J}_o^3}{\left(D_J V_t^2 k^2 + 3(2V_o - V_t)\mathcal{F}J_o^2 + V_t(V_t - V_o)\right)} \tag{3.11}$$

We know that for the parameters we fixed, $\mathcal{F}$ is negative, this is also apparent from the results obtained from the homotopy analysis method Fig[2.4], and so $V_o < V_t$.Hence the numerator in the third component of the dispersion relation is positive. Let's check the denominator for $k = 0$

$$3(2V_o - V_t)\mathcal{F}J_o^2 + V_t(V_t - V_o) \tag{3.12}$$

and J_o satisfies following relation

$$\mathcal{F}J_o^2 = \frac{V_o V_t - V_t^2}{2V_o - V_t}$$

using this in equation 3.12, we obtain

$$\begin{aligned} &3(V_o V_t - V_t^2) - V_o V_t + V_t^2 \\ &= 2(V_o V_t - V_t^2) < 0 \end{aligned}$$

Hence we most obtain unstable wave mode of wavenumber(k^*)

$$k^* = \sqrt{\frac{2(1 - V_o/V_t)}{D_J}}$$

We have $D_J = 9.70$and $V_t - V_o = \mathcal{F}J_o^2$
so

$$k^* = \sqrt{-\frac{2\mathcal{F}}{D_J V_t}} J_o$$

Where $\mathcal{F}$ is $O(10^8)$, $D_J V_t$ is $O(10^2)$ and J_o is $O(10^{-7})$, so k^* is $O(10^{-4})$ which implies that the wavelength is $O(10^4)$, which corresponds to the order of 1cm. Let's calculate exact values.
$\mathcal{F} = -3.03 \times 10^8$, $D_J = 9.70$, $V_t = 81.89$, $J_o = 1.67 \times 10^{-7}$,
which gives us $k^* = 1.46 \times 10^{-4}$
which corresponds to wavelength of 4.3×10^4, or 5.76 cm. Which is in variance with the experimentally observed, 0.16 cm.
Hence the two component model 3.10 fails to explain pattern formation in the given system. The result was expected as the models based on only NDR are in variance with the experimental observations.[7]
Another cause of instabilities in our system can be of thermal nature. We'll take into account the joule heating effect of the gas, and derive a three component reacting diffusion type model, with temperature being the third component.

3.2 Three component reaction diffusion type model

As observed from our work in previous chapter, change in temperature leads to change in the intrinsic scales of the system and can lead to instabilities. gas temperature can change in our system via joule heating of gas[13], which is described by

$$nc_p \partial_t T = \theta \nabla^2 T + \vec{J} \cdot \vec{E} \tag{3.13}$$

where n is the number density of gas, c_p is specific heat of gas at constant pressure, θ is thermal conductivity, and $\vec{J}, \vec{E}$ are electric current and electric field respectively. Equation 3.13 is subject to following boundary conditions

$$\begin{aligned} \textbf{At gas-semiconductor boundary:} \quad & T = T_o \\ \textbf{At other boundaries:} \quad & (\hat{n}_b \cdot \vec{\nabla}) T = 0 \end{aligned}$$

where $\hat{n}_b$ is unit vector perpendicular to the boundary wall. We have Dirichlet boundary condition at gas-semiconductor boundary because the temperature of semiconductor is maintained at a certain cryogenic value T_o, while Neumann boundary condition at the other boundaries is the no flux condition due to insulating walls.
Having described this, we'll now write the nondimensionalized form of Equation 3.13. Re-

ferring equation 1.3 for the intrinsic parameters we get

$$\mathcal{T}\partial_t T = D_T\nabla^2 T + \vec{\mathcal{J}}\cdot\vec{\mathcal{E}} \quad | \, \mathcal{T} = \frac{nc_p}{\tau\mathcal{E}_o^2 e\eta\mu_i} \quad D_T = \frac{\theta}{\xi^2\mathcal{E}_o^2 e\eta\mu_i} \tag{3.14}$$

We'll now average T axially(along x), this averaged out temperature will be used to scale the intrinsic parameters. Also we'll assume that only the axial component of current leads to gas heating. For the sake of simplicity we'll also divide the above equation with T_o. We arrive at

$$\mathcal{T}_T\partial_t\bar{T} = D_T L_x\partial_y^2\bar{T} - \frac{3D_T}{L_x}(\bar{T}-1) + \mathcal{J}_o V \quad | \, \mathcal{T}_T = \frac{nc_p T_o L_x}{\tau\mathcal{E}_o^2 e\eta\mu_i} \quad D_T = \frac{\theta T_o}{\xi^2\mathcal{E}_o^2 e\eta\mu_i} \tag{3.15}$$

where $\bar{T} = \widetilde{T}/T_o$

Let's see how temperature changes the intrinsic parameters of the system. Referring to the definitions of intrinsic parameter 1.3, and using the fact that $p \propto 1/\bar{T}$ we find that

$$\tau \propto \bar{T}^2 \quad \xi \propto \bar{T}$$
$$\mathcal{E}_o \propto \frac{1}{\bar{T}} \quad \eta \propto \frac{1}{\bar{T}^2}$$

We'll now express equations for current and voltage at semiconductor-gas boundary with new scaled intrinsic parameters. While 3.4 remains unchanged, but 3.9 modifies as

$$\begin{aligned}\mathcal{T}_J\partial_t\mathcal{J}_o =& \Big(\frac{V - V_t^o - (\frac{2V-V_t^o}{V_t})\mathcal{F}(\bar{T},\gamma,L_x)\mathcal{J}_o^2\bar{T}_o^6}{V_t^o}\Big)\mathcal{J}_o\bar{T} + D_J\bar{T}^2\partial_y^2\mathcal{J}_o \\ \mathcal{T}_J =& \frac{\Big(1-\big(\log(1+\gamma^{-1})\big)^{-1}\Big)L_x}{(1+\gamma)\log(1+\frac{1}{\gamma})}\end{aligned}$$

where $V_t^o = \frac{V_t}{\bar{T}}$ and $\mathcal{F}(\bar{T}, L_x, \gamma)$. We need to find out how $\mathcal{F}$ changes as a function of $\bar{T}$. Referring [11], if we neglect the logarithmic dependence of V_t on $\bar{T}$, we find $\mathcal{F} \sim \bar{T}^{-3}$. We do have an equation now to work with, but it is a bit messy, we'll assume that $\mathcal{J}_o^2$ is negligible, and we'll obtain

$$\begin{aligned}\mathcal{T}_J\partial_t\mathcal{J}_o =& \Big(\frac{V}{V_t} - \frac{1}{\bar{T}}\Big)\mathcal{J}_o\bar{T} + D_J\partial_y^2 J_o \\ \mathcal{T}_J =& \frac{\Big(1-\big(\log(1+\gamma^{-1})\big)^{-1}\Big)L_x}{\bar{T}^2(1+\gamma)\log(1+\frac{1}{\gamma})}\end{aligned} \tag{3.16}$$

and equation 3.15 remains unchanged on scaling the intrinsic parameters.

Equation 3.4, 3.16 and 3.15 gives a three component reaction diffusion model

$$
\begin{aligned}
\mathcal{T}_V \partial_t V = V_o - V - \frac{L_x^s}{\sigma}\mathcal{J}_o + (L_x^s)^2 \partial_y^2 V \quad &\Big| \quad \mathcal{T}_V = \frac{L_x^s}{\sigma}\Big(\frac{1}{L_x} + \frac{\epsilon_{sem}}{L_x^s}\Big) \\
\mathcal{T}_J \partial_t \mathcal{J}_o = \Big(\frac{V}{V_t} - \frac{1}{\bar{T}}\Big)\mathcal{J}_o + D_J \partial_y^2 J_o \quad &\Big| \quad \mathcal{T}_J = \frac{\Big(1 - \big(\log(1+\gamma^{-1})\big)^{-1}\Big)L_x}{\bar{T}^2(1+\gamma)\log(1+\frac{1}{\gamma})} \\
\mathcal{T}_T \partial_t \bar{T} = D_T L_x \partial_y^2 \bar{T} - \frac{3D_T}{L_x}(\bar{T} - 1) + \mathcal{J}_o V \quad &\Big| \quad \mathcal{T}_T = \frac{n c_p T_o L_x}{\tau \mathcal{E}_o^2 e \eta \mu_i} \\
&\quad D_T = \frac{\theta T_o}{\xi^2 \mathcal{E}_o^2 e \eta \mu_i}
\end{aligned}
\tag{3.17}
$$

For the parameters(i.e parameters at which the experiments[19]) we are working with, the timescales have following values

$$
\begin{aligned}
\mathcal{T}_V &= 1.2 \times 10^5 \\
\mathcal{T}_J &= 45.7 \\
\mathcal{T}_T &= 8.2 \times 10^4
\end{aligned}
\tag{3.18}
$$

Linear stability analysis

As apparent from the timescales Eq[3.18], $\mathcal{T}_J/\mathcal{T}_V \ll 1$ the dynamics of current density occurs at much faster rate as compared to voltage and temperature. Assuming that $\mathcal{T}_J/\mathcal{T}_V \approx 0$, we'll drop the time derivatives in the governing equation for current density.
We study the growth of perturbations about homogeneous solution$(\tilde{V}, \tilde{\mathcal{J}}_o, \tilde{\bar{T}})$.

$$
\begin{aligned}
\mathcal{J}_o &= \tilde{\mathcal{J}}_o + \delta\mathcal{J} e^{\omega t} e^{iky} \\
V &= \tilde{V} + \delta V e^{\omega t} e^{iky} \\
\bar{T} &= \tilde{T} + \delta T e^{\omega t} e^{iky}
\end{aligned}
$$

We obtain coupled linear equations,

$$\omega\delta V = -\delta V - \frac{L_x^s}{\sigma}\delta\mathcal{J}_o - \frac{(L_x^s)^2}{2}k^2\delta V$$
$$0 = \delta V\frac{\mathcal{J}_o}{V_t} + \frac{\mathcal{J}_o\delta\bar{T}}{\bar{T}^2} - D_J k^2\delta\mathcal{J}_o$$
$$\frac{\mathcal{T}_\mathcal{T}}{\mathcal{T}_\mathcal{V}}\omega\delta T = \delta\mathcal{J}_o V + \mathcal{J}_o\delta V - D_T L_x k^2\delta T - \frac{3D_T}{L_x}\delta T$$

solving these equations we run into eigenvalue problem, which provides us with dispersion relation, $\omega(k)$, which has a positive maxima at $k = 0.0118$(Fig:3.2) which corresponds to the wavelength of 0.071 cm, which is variance with the numerically observed 0.11 cm and experimentally observed 0.16 cm[13].

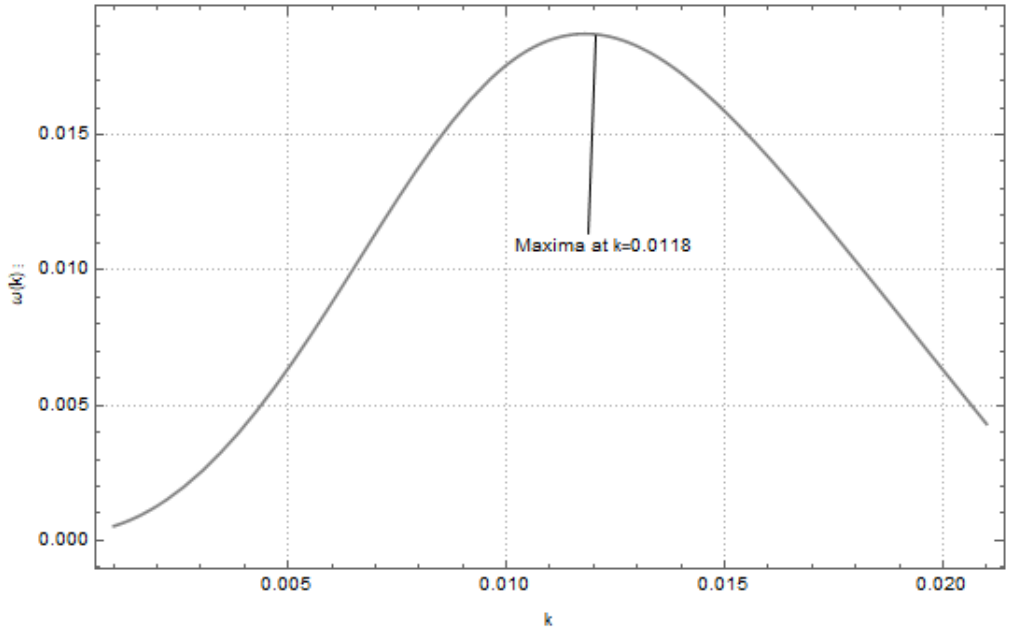


Figure 3.2: Dispersion relation obtained from the linear stability analysis of the model 3.17

The three component model based on thermal instability doesn't reproduce the experimental results. While the model is linearly unstable to a patterned state, but the wave number of the pattern state is different from the experimentally observed state.
The model described in [12] gives a closer description to the experimental observations. The difference from the model described in [12] and the one we derived is that we assumed that the change current voltage characteristic is purely thermal, while we ignored space charge

effects.

We'll try to perform linear stability analysis on the three component model which incorporates NDR instability.

$$\begin{aligned}
\mathcal{T}_V \partial_t V = V_o - V - \frac{L_x^s}{\sigma}\mathcal{J}_o + (L_x^s)^2 \partial_y^2 V \quad &\Big| \quad \mathcal{T}_V = \frac{L_x^s}{\sigma}\Big(\frac{1}{L_x} + \frac{\epsilon_{sem}}{L_x^s}\Big) \\
\mathcal{T}_J \partial_t \mathcal{J}_o = \Big(\frac{V}{V_t} - \frac{1}{\bar{T}} - (\frac{2V}{V_t^2}T^2 - \frac{T}{V_t})\mathcal{F}\mathcal{J}_o^2\mathcal{T}^2\Big)\mathcal{J}_o + D_J \partial_y^2 J_o \quad &\Big| \quad \mathcal{T}_J = \frac{\Big(1 - \big(\log(1+\gamma^{-1})\big)^{-1}\Big)L_x}{\bar{T}^2(1+\gamma)\log(1+\frac{1}{\gamma})} \\
\mathcal{T}_T \partial_t \bar{T} = D_T L_x \partial_y^2 \bar{T} - \frac{3D_T}{L_x}(\bar{T} - 1) + \mathcal{J}_o V \quad &\Big| \quad \mathcal{T}_T = \frac{nc_p T_o L_x}{\tau \mathcal{E}_o^2 e\eta\mu_i} \\
&\qquad D_T = \frac{\theta T_o}{\xi^2 \mathcal{E}_o^2 e\eta\mu_i}
\end{aligned} \tag{3.19}$$

Performing linear stability analysis on [Eq:3.19], we obtain, $k^* = 0.0134$, which corresponds to wavelength of 0.063 cm. This is again in variance with the observations.

We have mentioned previously that D_J was chosen as suggested in [12]. Since, this diffusion coefficient is the only term we haven't derived, we'll try to vary this coefficient and study the model.

Another important point to note is that the equation describing the dynamics of current at cathode [Eq:3.7] is based on the assumption that only the electrons at cathode-semiconductor boundary are responsible for subsequent multiplication of charge carriers, which isn't true, and might not be a good approximation.

We would like to highlight that equation 3.7 requires a bit more critiquing and must be validated numerically.

Chapter 4

Conclusion

In this concluding chapter, we'll highlight the results and outcomes of the work done. And provide with some direction for future work.

Key Results

- The thesis presents a new numerical technique based on the Homotopy analysis method to solve drift-diffusion model of gas discharge. We were able to obtain, Current-Voltage-Temperature plot Fig[2.7], which showcases the thermal and negative differential conductivity instabilities in the system. While the new technique qualitatively replicates the expected behaviour, a much more careful analysis is required to present a useful technique.

- Two component reaction diffusion model 3.10(consisting of potential and axial component of current at gas semi-conductor boundary) was derived, and was shown to be linearly unstable to perturbations at the parameters we expect a patterned state, however the wavelength observed was significantly different from the experimentally observed

- A three component reaction diffusion type model 3.17, an extension of the two component model, was derived, and was shown to be linearly unstable to the perturbations, but the wavelength obtained is in variance with the experimentally observed. Only thermal instability was taken into account in the model. A more accurate model is de-

veloped by including NDR as an instability, to the model 3.17, however, still the model doesn't replicate the expected behaviour, i.e the obtained wavelength from the linear stability analysis is in variance with the experimentally and the numerically observed.

A rather significant amount of time was spent on numerical simulations of the experiment[19]. But to no avail. We'll give a description of the numerical techniques which were attempted and the problems faced in the Appendix.

Directions for future work

- Numerical techniques based on the homotopy analysis method in order to simulate gas discharges in a much larger parameter space can be developed.
- Formalising the homotopy analysis technique for solving the drift diffusion model and providing with a more rigorous description.
- Numerical simulations of the dynamical patterns, have never been reported from first principles, i.e the drift diffusion model, and it is a major challenge. The huge difference in the time scales and the highly non-equilibrium nature of cold plasma posits a computational challenge.
- We have criticized the derivation of the equation governing the dynamics of total current at cathode-semiconductor boundary in previous chapter. Numerical simulations are required to verify the validity of equations and if necessary to come up with better description.

Appendix

Numerical simulations

In order to verify our analytical work, we also attempted to simulate gas discharges. Given the highly non-linear and coupled nature of the model equations, the numerical techniques are prone to instabilities. Majority of the time of the project was spent in experimenting with different techniques which worked and were computationally efficient. We attempted to simulate drift diffusion model, and drift diffusion model coupled to joule heating equation.

The case of direct methods

We are interested in the stationary solutions of the equations, hence in the first attempt we dropped of the time derivatives, and attempted to solve the coupled set of equations simultaneously. We discretized the continuous variables and attempted to solve the obtained linear set of equations via matrix inversion.
But the matrix solvers returned an error hinting towards the fact that the matrix is *numerically singular*, and hence the matrix can't be inverted.
This can be rationalized by the fact that the model is under-determined. We have a boundary condition on electron density profile at gas-semiconductor boundary, which is dependent on ion density at that boundary.
So we'll stick to transient analysis, where we give an initial guess and evolve the system till desired convergence is reached. Equations are solved sequentially.

Explicit vs Implicit techniques

One may use explicit or implicit techniques to solve the partial differential equations numerically. While explicit methods are much simpler to implement, they may have stability issues and the descritization has to satisfy CFL conditions. Which greatly increases the computational time. In our model, we have to have huge number of iterations($O(10^{10})$), while keeping fine descritization and satisfying the CFL condition. So, we'll work with implicit techniques.

Numerical simulations of drift diffusion model gas discharges

We attempted to numerically solve the non dimensionalized model described in 1.3. Implicit or semi-implicit techniques were used and particle density flux was discretized via finite volume methods.

Semi-implicit scheme to solve Poisson's equation

For the semi-implicit scheme $-\nabla^2\mathcal{V} = \rho_i - \mu\rho_e$ is discretized as

$$\begin{aligned}&(1 + \Delta t(\rho_i + \rho_e))\nabla^2 V + \Delta t(\vec{\nabla}(\rho_i + \rho_e) \cdot \vec{\nabla} V = \\ &(\rho_i - \mu\rho_e) + \Delta t D_e \nabla^2 \rho_e - \Delta t D_i \nabla^2 \rho_i\end{aligned} \tag{4.1}$$

where the spatial derivatives are approximated by first order center difference approximations. We solve for V at $t + \Delta t$ while ρ_i, ρ_e are at t

Scharfetter-Gummel scheme

We use finite volume method to solve continuity equations numerically. In finite volume method we integrate the differential equations over a finite volume. In continuity equation we have divergence of flux, and integrating over a finite volume, we require the flux values at the boundaries of finite volume.

We used Scharfetter-Gummel method as described in [13] to estimate flux at the boundaries. We will use regular square mesh.
The obtained linear equations were solved via direct sparse matrix solver, MUMPS. Iterative methods like Alternating Direction Implicit method and SOR methods were also attempted but they failed and were occasionally computationally inefficient as the rate of convergence was very slow.

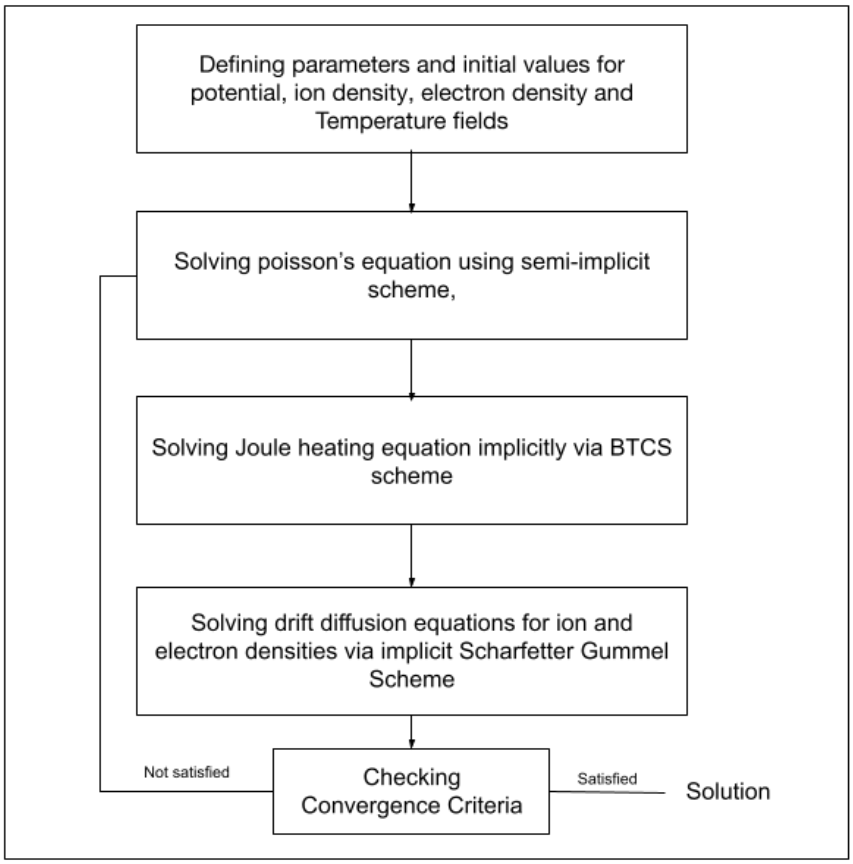


Figure 4.1: Numerical scheme

However, we were not able to obtain stationary solutions using the above scheme. The variables were evolved for a certain number of iterations, but eventually the system became unstable.

Results

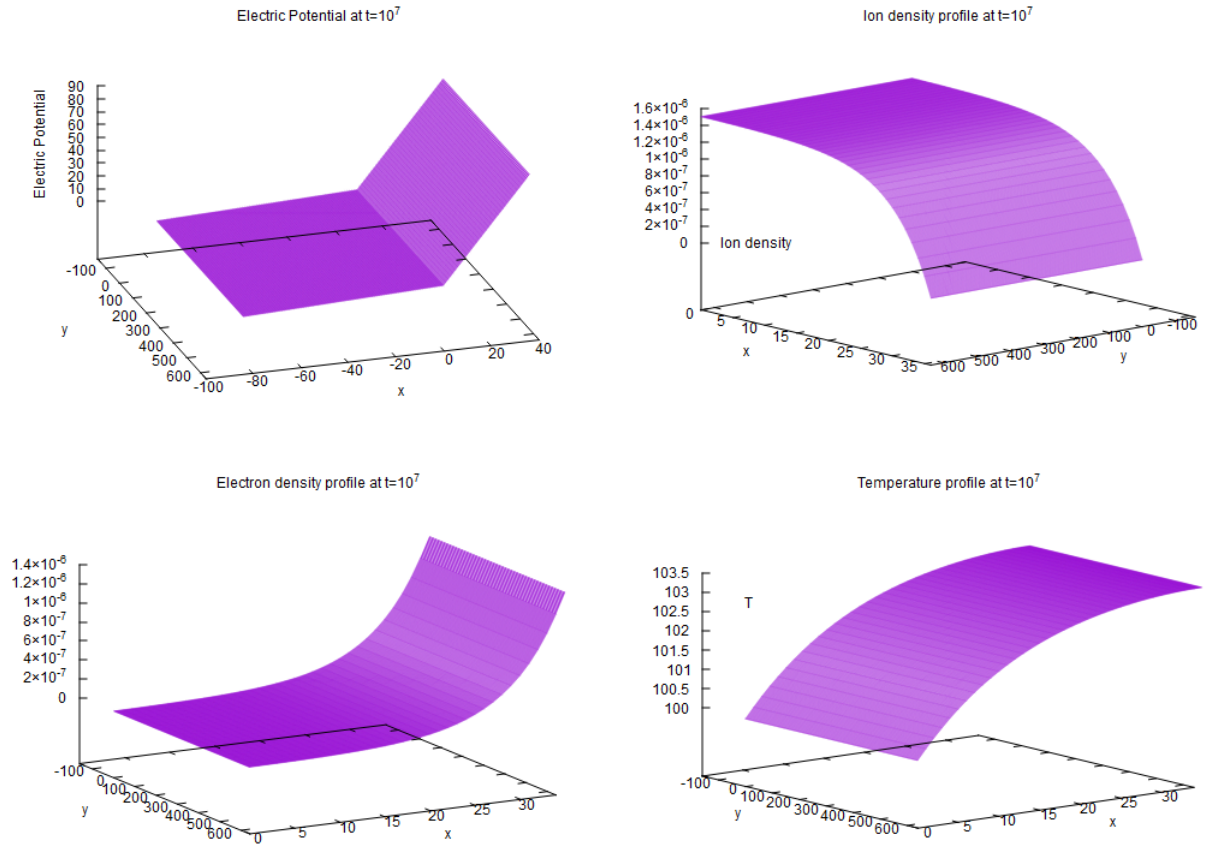


Figure 4.2: Results from transient numerical solutions of Drift-Diffusion model of gas discharges coupled to Joule heating equation at $t = 10^7$(dimensionless)

Fig 4.2 shows the results of numerically solving the model for $t = 10^7$. The results here match qualitatively match the homogeneous profiles expected at the given parameters.[19]. After $t \approx 3.5 \times 10^7$, the system become unstable and numerical values of the profiles become undefined. This may be attributed to the fact that we are violating the CFL condition while solving the model for accelerating computation. Since we are using implicit techniques, the constraint from CFL condition is not strong and violating it shouldn't necessarily affect the solution. However in our case it does. The possible solution to this is adaptive time stepping techniques. We'll work on developing proper numerical techniques to simulate gas discharges in future.

Calculation of $\mathcal{F}$ using perturbative techniques

Given the following model

$$\begin{aligned} \partial_x \mathcal{J}_i &= (\mathcal{J}_{total} - \mathcal{J}_i)\exp(-\frac{1}{\mathcal{E}}) \\ \partial_x^2(\mathcal{E}^2) &= 2\mathcal{J}_i \end{aligned} \tag{4.2}$$

with the following boundary conditions

$$\begin{aligned} \textbf{At cathode(x=L)} \quad & \mathcal{J}_i = \frac{\mathcal{J}_{total}}{(1+\gamma)} \qquad \mathcal{V} = -V_o \\ \textbf{At anode(x=0)} \quad & \mathcal{J}_i = 0 \qquad\qquad\quad \mathcal{V} = 0 \end{aligned} \tag{4.3}$$

we can use perturbative techniques to solve the model defined above. Choosing $\mathcal{J}_{total}$ as perturbation parameter, we write following ansatz

$$\begin{aligned} \mathcal{J}_i &= \sum_{i=1}^{\infty} (\mathcal{J}_{total})^i j_i(x) \\ \mathcal{E} &= \sum_{i=0}^{\infty} (\mathcal{J}_{total})^i E_i(x) \end{aligned}$$

Again the boundary condition on ion flux at cathode, give the following condition

$$\exp\Big(-\int_0^L dx \exp(-\frac{1}{\mathcal{E}})\Big) = \frac{\gamma}{1+\gamma}$$

Solving at zeroth order we obtain Townsend solution for electric field which satisfies the above relation.

$$\exp\Big(-\int_0^L dx \exp(-\frac{1}{E_o})\Big) = \frac{\gamma}{1+\gamma}$$

so we have constraints on E_i at each order of calculation.

$$\exp\Big(-\int_0^L dx \exp(-\frac{1}{\mathcal{E}})\Big) = \exp\Big(-\int_0^L dx \exp(-\frac{1}{E_o})\Big) + \sum_{i=1}^{\infty} (\mathcal{J}_{total})^i C_i$$

where $C_i = 0$ Using these we obtain that

$$\int_0^L E_1(x)dx = 0$$

and

$$\int_0^L E_2(x)dx = -\frac{\frac{1}{E_o^4} - \frac{2}{E_0^3}}{\frac{1}{E_o^2}} \int_0^L (E_1(x))^2 dx$$

calculating $E_1(x)$ via the constraints described above, we obtain

$$V = V_T - \frac{\frac{1}{E_o^4} - \frac{2}{E_0^3}}{\frac{1}{E_o^2}} (\mathcal{J}_{total})^2 \int_0^L (E_1(x))^2 dx + O((\mathcal{J}_{total})^3)$$

Hence $\mathcal{F}$ is given by

$$\mathcal{F} = -\frac{\frac{1}{E_o^4} - \frac{2}{E_0^3}}{\frac{1}{E_o^2}} \int_0^L (E_1(x))^2 dx$$

where $E_1(X)$ is calculated from equation

$$E_o \partial_x E_1 = 1 - \exp\big(- x \exp(-1/E_o)\big)$$

subject to constraint

$$\int_0^L E_1(x)dx = 0$$

Bibliography

[1] Sh S Kasymov, LG Paritskii, and SM Ryvkin. Investigation of ionization-type image converter. *Deposited in VINITI*, (2693), 1974.

[2] Yu A Astrov and Yu A Logvin. Formation of clusters of localized states in a gas discharge system via a self-completion scenario. *Physical Review Letters*, 79(16):2983, 1997.

[3] Yu Astrov, E Ammelt, S Teperick, and H-G Purwins. Hexagon and stripe turing structures in a gas discharge system. *Physics Letters A*, 211(3):184–190, 1996.

[4] Yu A Astrov, I Müller, E Ammelt, and H-G Purwins. Zigzag destabilized spirals and targets. *Physical review letters*, 80(24):5341, 1998.

[5] HU Bödeker, MC Röttger, AW Liehr, TD Frank, R Friedrich, and H-G Purwins. Noise-covered drift bifurcation of dissipative solitons in a planar gas-discharge system. *Physical Review E*, 67(5):056220, 2003.

[6] C Strümpel, H-G Purwins, and Yu A Astrov. Spatiotemporal filamentary patterns in a dc-driven planar gas discharge system. *Physical review E*, 63(2):026409, 2001.

[7] Danijela D Šijačić, Ute Ebert, and Ismail Rafatov. Period doubling cascade in glow discharges: Local versus global differential conductivity. *Physical Review E*, 70(5):056220, 2004.

[8] Ismail R Rafatov, Danijela D Šijačić, and Ute Ebert. Spatiotemporal patterns in a dc semiconductor-gas-discharge system: Stability analysis and full numerical solutions. *Physical Review E*, 76(3):036206, 2007.

[9] Marat Akhmet, Ismail Rafatov, and Mehmet Onur Fen. Extension of spatiotemporal chaos in glow discharge-semiconductor systems. *Chaos: An Interdisciplinary Journal of Nonlinear Science*, 24(4):043127, 2014.

[10] H-G Purwins, HU Bödeker, and Sh Amiranashvili. Dissipative solitons. *Advances in Physics*, 59(5):485–701, 2010.

[11] Danijela D Šijačić and Ute Ebert. Transition from townsend to glow discharge: Subcritical, mixed, or supercritical characteristics. *Physical Review E*, 66(6):066410, 2002.

[12] Yu P Raizer and MS Mokrov. A simple physical model of hexagonal patterns in a townsend discharge with a semiconductor cathode. *Journal of Physics D: Applied Physics*, 43(25):255204, 2010.

[13] MS Mokrov and Yu P Raizer. Simulation of current filamentation in a dc-driven planar gas discharge–semiconductor system. *Journal of Physics D: Applied Physics*, 44(42):425202, 2011.

[14] MS Mokrov and Yu P Raizer. 3d simulation of hexagonal current pattern formation in a dc-driven gas discharge gap with a semiconductor cathode. *Plasma Sources Science and Technology*, 27(6):065008, 2018.

[15] I Rafatov, EA Bogdanov, and AA Kudryavtsev. On the accuracy and reliability of different fluid models of the direct current glow discharge. *Physics of Plasmas*, 19(3):033502, 2012.

[16] Shijun Liao. Homotopy analysis method: a new analytical technique for nonlinear problems. *Communications in Nonlinear Science and Numerical Simulation*, 2(2):95–100, 1997.

[17] Shijun Liao. *Beyond perturbation: introduction to the homotopy analysis method*. CRC press, 2003.

[18] Shijun Liao. Notes on the homotopy analysis method: some definitions and theorems. *Communications in Nonlinear Science and Numerical Simulation*, 14(4):983–997, 2009.

[19] Yu A Astrov, AN Lodygin, and LM Portsel. Hexagonal structures of current in a "semiconductor-gas-discharge gap" system. *Technical Physics*, 56(2):197–203, 2011.

[20] Yuri P Raizer and John E Allen. *Gas discharge physics*, volume 2. Springer Berlin, 1997.

[21] Yu P Raizer, EL Gurevich, and MS Mokrov. Self-sustained oscillations in a low-current discharge with a semiconductor serving as a cathode and ballast resistor: Ii. theory. *Technical physics*, 51(2):185–197, 2006.